REPORT DOCUMENTATION PAGE

1a. REPORT SECURITY CLASSIFICATION UNCLASSIFIED	1b. RESTRICTIVE MARKINGS None.
2a. SECURITY CLASSIFICATION AUTHORITY	3. DISTRIBUTION/AVAILABILITY OF REPORT Unrestricted
2b. DECLASSIFICATION/DOWNGRADING SCHEDULE	

DISTRIBUTION STATEMENT A
Approved for public release
Distribution Unlimited

4. PERFORMING ORGANIZATION REPORT NUMBER(S) GITAER-EAD 95-7	5. MONITORING ORGANIZATION REPORT NUMBER(S) AFOSR-TR-96-0013

6a. NAME OF PERFORMING ORGANIZATION Georgia Tech Research Corporation	6b. OFFICE SYMBOL (If applicable)	7a. NAME OF MONITORING ORGANIZATION SAME AS #8

6c. ADDRESS (City, State and ZIP Code) Georgia Institute of Technology School of Aerospace Engineering, Atlanta Georgia 30332-0150	7b. ADDRESS (City, State and ZIP Code) SAME

8a. NAME OF FUNDING/SPONSORING ORGANIZATION AFOSR	8b. OFFICE SYMBOL (If applicable) NA	9. PROCUREMENT INSTRUMENT IDENTIFICATION NUMBER F49620-93-1-0036

8c. ADDRESS (City, State and ZIP Code) AFOSR/NA, 110 Duncan Avenue, Suite B115 Bolling AFB, DC20332-0001	10. SOURCE OF FUNDING NOS.

PROGRAM ELEMENT NO.	PROJECT NO.	TASK NO.	WORK UNIT NO.
61102F	2307	AS	

11. TITLE (Include Security Classification)
QUASI-PERIODICITY IN VORTEX FLOWS   (U)

12. PERSONAL AUTHOR(S)
Komerath, N.M., Hubner, J.P., Dixon, C.J.

13a. TYPE OF REPORT FINAL TECHNICAL	13b. TIME COVERED FROM 11/92 TO 9/95	14. DATE OF REPORT (Yr., Mo., Day) 1995 October 13	15. PAGE COUNT 60

16. SUPPLEMENTARY NOTATION

17. COSATI CODES			18. SUBJECT TERMS (Continue on reverse if necessary and identify by block number)
FIELD	GROUP	SUB. GR.	VELOCITY FLUCTUATIONS, VORTEX FLOWS

19. ABSTRACT (Continue on reverse if necessary and identify by block number)

Part 1 summarizes the search for the origin and nature of nearly-periodic velocity fluctuations observed over fighters at incidence angles between 15 and 40 deg. The Strouhal number and spectral shape remain constant over a wide range of Reynolds number, but vary with incidence and sweep. A 1/32-scale F-15 and a 59.3-deg. cropped delta flat plate are used for detailed studies, but the phenomenon is general to leading-edge vortex flows. Empirical correlations are developed for various aircraft configurations and wing planforms. Cross-spectral analysis traced the fluctuations upstream along a helical path to the surface. Streaklines and laser velocimetry discovered spanwise counter-rotating structures in the surface shear region under the vortex, amplifying downstream. Remaining hypotheses are based on centrifugal instability and unsteady vortex-surface interaction. Surface mini-fences modified and attenuated the spectra by as much as 50%, reinforcing the finding of amplification from the surface layer. Part 2 details improvements to the High Angle of Attack Stability and Control code predicting swept-wing configuration aerodynamics. Effects of camber, edge bevels, and of multiple vortices on vortex loads and breakdown are accurately predicted, as well as the turbulent vortex core size.

20. DISTRIBUTION/AVAILABILITY OF ABSTRACT UNCLASSIFIED/UNLIMITED ☒ SAME AS RPT. ☐ DTIC USERS ☐	21. ABSTRACT SECURITY CLASSIFICATION Unclassified

NAME OF RESPONSIBLE INDIVIDUAL DR SAKELL	22b. TELEPHONE NUMBER (Include Area Code) 202-767-4935	22c. OFFICE SYMBOL AFOSR/NA

DD FORM 1473, 83 APR   EDITION OF 1 JAN 73 IS OBSOLETE.

DTIC QUALITY INSPECTED 1

TABLE OF CONTENTS

1. EXECUTIVE SUMMARY

1.1 Introduction

Beginning in November 1992, this project studied the origin and nature of the quasi-periodic velocity fluctuations which are observed over twin-tailed fighters at angles of attack between 15 and 40 degrees. Most of the results obtained have already appeared in published papers, which are listed in this report. An overview of the project is provided in this report. The doctoral thesis of J. Paul Hubner (Ref. 1) provides a detailed and comprehensive description.

Twin-tail buffeting problems are usually attributed to the bursting of strong vortices, and the resulting high-intensity turbulence. However, there is another insidious phenomenon which can drive tail vibrations and cause fatigue cracks on tails. Here the vibrations are driven by quasi-periodic flow fluctuations of relatively small amplitude, whose frequencies lock in with structural modes. Experiments show these fluctuations originating in the vortex flow over swept wings, and amplifying downstream. We studied these phenomena in detail to understand, predict and learn to suppress these fluctuations. We report the detailed search which identified the origin and nature of these fluctuations. Finally, we demonstrate that our hypothesis leads to success in attenuating these fluctuations.

1.2 Structure of the Project

The primary thrust of the project, summarized in Part 1 of the report, is to identify the origin and nature of the quasi-periodic velocity fluctuations on swept-winged configurations. Part 2 describes work under a subcontract to Mr. Charles Dixon, funded from AFWAL, to develop the High Angle of Attack Stability and Control (HASC) code for semi-empirical prediction of the vortex-flow aerodynamics of aircraft configurations. The work on this subcontract was closely tied to the Part 1 through exchange of experimental data and predictions.

1.3 Project Objectives

The objectives stated in the 1992 proposal were:

"A. Experimentally capture the origins, dominant features and fundamental mechanisms responsible for the quasi-periodic fluctuations in separating vortex flows.

B. Use knowledge of the flow mechanisms to try to suppress these fluctuations.

C. Use the measurements to refine current semi-empirical models for vortex behavior, and develop passive control strategies.

D. Using generic shapes and systematic experiments, explore prediction methods for the critical frequencies. Refine the predictions using available flight data.

E. Determine how the observed phenomena and control strategies are changed by finite-rate model acceleration in pitch, roll and yaw. Extend this to coupled pitch/roll. "

The project was proposed for 3 years. Funding was provided for two years. Objectives A, B and C were achieved, as detailed in this report. Objective D was partially met: empirical predictions were developed for several existing combat aircraft models and their corresponding flat-plate wing planforms, and these data were supplied to the manufacturers and Air Force Lab scientists. Whether these have been tested against flight test data is unknown. Objective E was deferred until a multiple-degree of freedom Wind Driven Dynamic Manipulator, invented at Georgia Tech under an Augmentation Grant from AFOSR (Ref. 2), becomes fully operational.

1.4 Status at the End of the Project

At present, we believe that the fluctuations arise due to an instability of the shear layer close to the wing surface, beginning at about 1/3 of the root chord downstream from the apex. The observed structures obey the descriptions of centrifugal instability, quantitatively demonstrating the counter-rotating structures typical of such instability. These structures amplify as the bottom of the vortex flow goes over the wing surface, where the local flow direction has a large spanwise component, and then go around the vortex periphery in a helical trajectory. Specifically, the fluctuations arise near the surface, not in the pre-breakdown or post-breakdown core region of the vortex as postulated by other researchers. The dominant frequency can be predicted from empirical correlations on scale models. Variations with angle of attack and leading edge sweep are predictable to a lesser degree from correlation formulae. Configuration details such as the fuselage do affect the frequency correlation, though they are not dominant. Accurate prediction of frequency is needed for precise identification of the structural models which are likely to resonate at each flight condition: this still needs scale model tests on detailed configurations. Applying very small "fences" on the surface is effective in modifying the amplitude of fluctuations in the entire vortex flow, with net overall reductions of up to 50% observed in experiments before any optimization of passive control is attempted. Active suppression techniques have not yet been attempted. With the nature of the phenomenon identified, and empirical correlations in hand, there is an excellent opportunity to learn to predict the fluctuation frequency in precise detail using computational studies, and to suppress the fluctuations using active and passive surface flow control techniques.

1.5. Degrees And Publications

Degrees Granted

Hubner, J.P., PhD in Aerospace Engineering, August 1995.

Klein, M., M.S. in Aerospace Engineering, August 1993.

Publications

1. Hubner, J.P., Komerath, N.M., "Spectral Mapping of Quasiperiodic Structures in a Vortex Flow." Journal of Aircraft, Vol.32, No. 3, May-June 1995, pp. 493-500.

2. Hubner, J.P., "An Investigation of Quasiperiodic Structures in the Vortical Flow Over Delta Wing Configurations". PhD Thesis, School of Aerospace Engineering, Georgia Institute of Technology, August 1995.

3. Hubner, J.P., Komerath, N.M., "Coherence-tracking of quasi-periodic structures in a vortex flow.". AIAA Paper 93-2914, 24th Fluid Dynamics Conference, Orlando, July '93.

4. Hubner, J.P., Komerath, N.M., "Visualization Of Quasi-Periodic Structures In A Vortex Flow". AIAA Paper 94-0624, Aerospace Sciences Meeting, Reno, Nevada, Jan. 94.

5. Klein, M.A., Hubner, J.P., Komerath, N.M., "Spectral Measurements in Vortex Flow over Swept-Winged Configurations at High Angle of Attack". AIAA Paper 94-1804, 12th Applied Aerodynamics Conference, Colorado Springs, Co., June 1994

6. Dixon, C.J., "Semi-Empirical Analysis of Vortex Breakdown with Aerodynamic and Buffet Effects". AIAA 94-3483, 1994.

7. Hubner, J.P., Komerath, N.M., "Modification of Spectral Characteristics in a Vortex Flow Field". AIAA 95-1795, Applied Aerodynamics Conference, San Diego, June '95.

8. Komerath, N.M., "Development of Narrow-Band Velocity Fluctuations in Vortex Flows". Invited paper. AIAA 95-2304, 26th Fluid Dynamics Conference, San Diego, June '95.
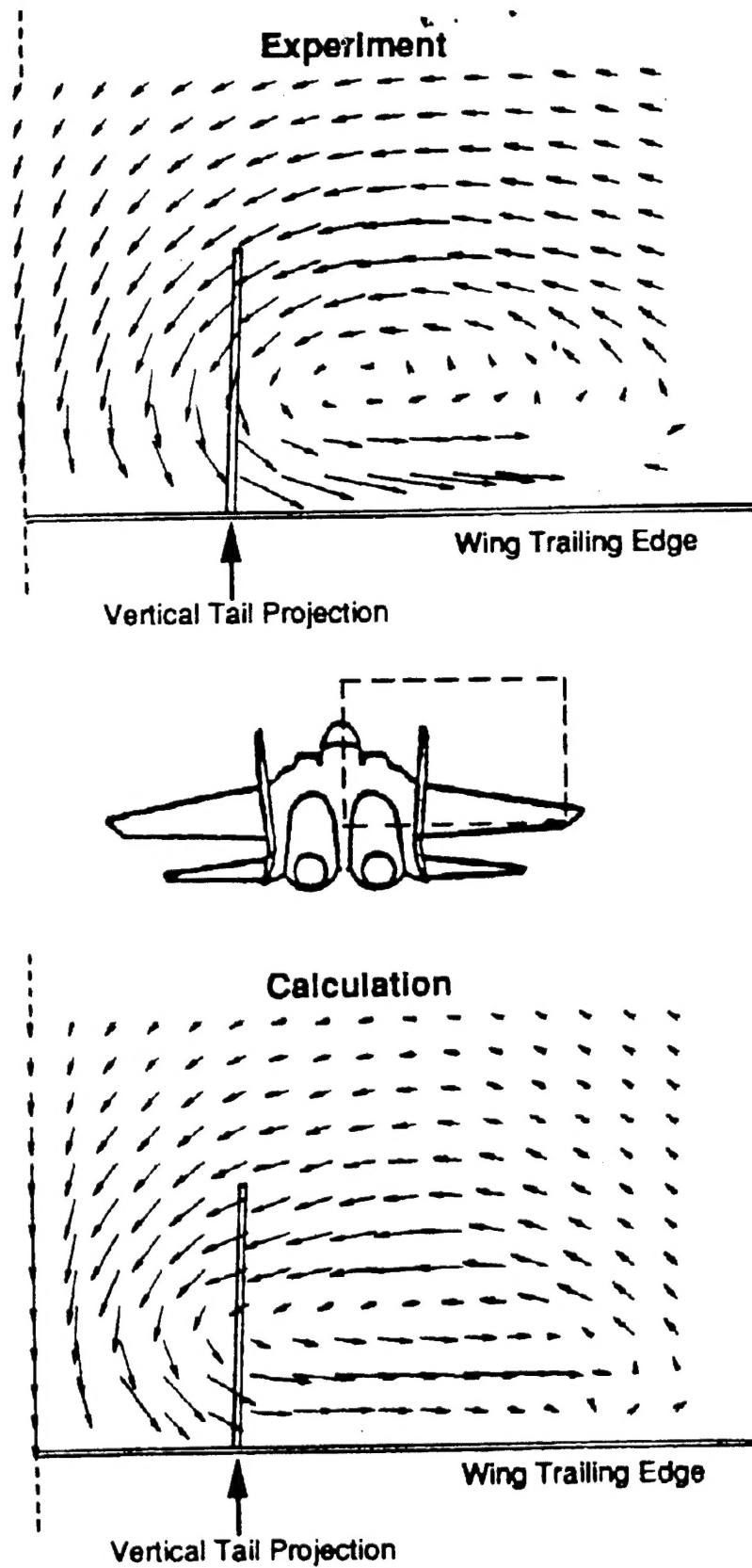
Figure 1: Measured and computed time-averaged cross-flow velocity field at the wing trailing edge plane of a 1/32-scale F-15 at $\alpha = 20$ deg.; Mach 0.1 (Ref. 4)

2. TECHNICAL SUMMARY, PART 1:
QUASI-PERIODIC VELOCITY FLUCTUATIONS IN VORTEX FLOW

2.1 Nomenclature

b	=	wing span
c	=	root chord
c_{mac}	=	mean aerodynamic chord
f	=	frequency, cycles per second
G()	=	nondimensionalized autospectral intensity function
n	=	reduced frequency
U_∞	=	freestream speed
α	=	angle-of-attack
β	=	angle between the root chord and a surface ray originating from the apex
Λ	=	wing leading-edge sweep
ϕ	=	phase of cycle
θ	=	angle between the root chord and a ray originating from the apex in the vertical plane

2.2 Introduction

In the late 1980s, a project at our laboratory aimed to define the environment of twin vertical tails at high angles of attack in order to help improve design specifications for future aircraft. The flow around a 1/32-scale F-15 was visualized using tufts and laser sheets, and the velocity field at $\alpha = 20$ deg. was mapped using laser velocimetry[3]. The time-averaged results were verified against a Navier-Stokes solver[4]. Fig. 1 shows some of the features. This is post-breakdown flow. The vortex core "bursts" essentially at the apex at this angle of attack. Strong vortex cores are thus not visible in this flow anywhere over the wings, unlike the flow over an F/A-18 with its highly swept leading-edge extensions. In fact our experiments were aimed at detecting such vortices and the trajectory of the expected high-turbulence region: our complete failure to detect any such feature forced deeper studies of the problem.

Autospectra of velocity fluctuations were measured over a rigid model using hot-film anemometer sensors. These gave the frequency distribution of the fluctuation energy near the tails. The prevailing model of tail vibrations was that of a structure responding to "broadband turbulence". The hot-film spectral results were a surprise. Fig. 2[5] shows a small spectral peak beginning over the wing surface, then amplifying, shifting lower in frequency, and finally focusing most of the energy of the fluctuations into a dominant, narrow frequency band enveloping the upper half of the vertical tails. Thus it appeared that tail vibrations might be
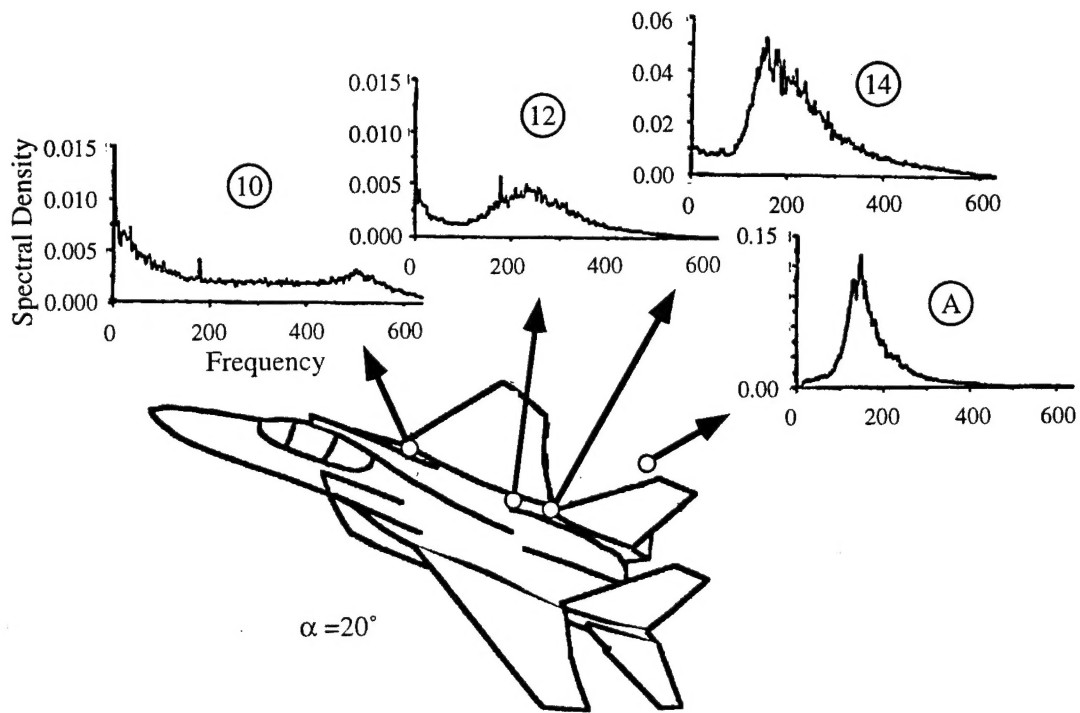
Figure 2: Hot-film velocity spectra measured above a 1/32-scale F-15 at 33 m/s (Ref. 5)
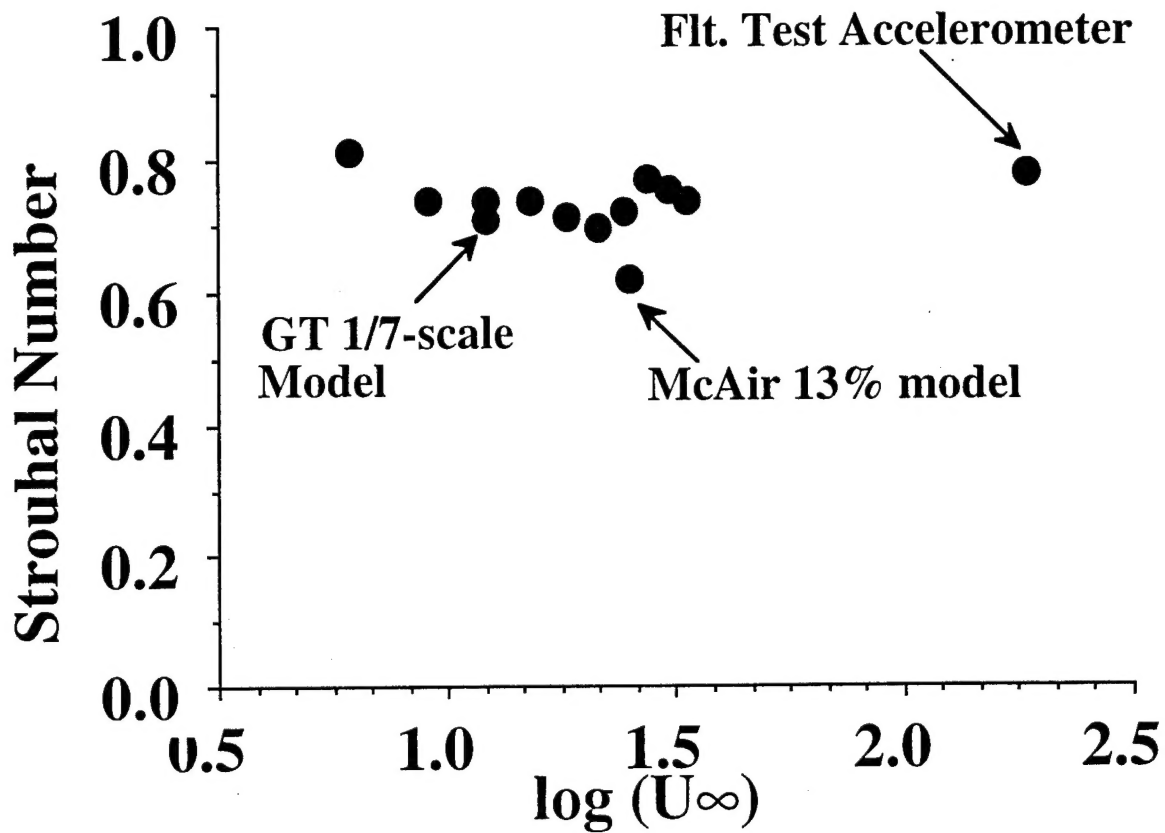
Figure 3: Strouhal number of velocity fluctuations based on wing mean aerodynamic chord, measured at the vertical tail top of F-15 scale models at $\alpha = 20$ deg. and compared with flight test accelerometer data. From Ref. 5.

"driven" at a very well-defined frequency, amenable to smart techniques for reducing these vibrations if the phenomenon is understood.

In the rest of the report, we use f_{Pk} to denote the frequency of the spectral peak. The spectrum of velocity fluctuations does rise to a sharp peak in most cases. Sometimes, two closely-spaced peaks are seen. Where there is uncertainty about the peak, we use a "moving window average" of three successive frequency intervals to determine the frequency of the spectral peak from experimental data. The Strouhal number computed using this frequency, freestream velocity and some length scale of the model is of most interest:

$$\mathbf{n} = f_{Pk} L / U_{\infty} . \qquad\qquad (1)$$

Fig. 3 shows that $f_{Pk}L$ for the F-15 scales with U_{∞}, all the way from wind-tunnel tests at 7 to 33 m/s on a 1/32-scale model, past tests of a 1/7-scale model at 13 m/s and 13% scale model at about 28 m/s (Ref. 6), and matches the frequency of the tail *vibrations* measured at the top of a full-scale aircraft tail at Mach 0.6. This spans three orders of magnitude in Reynolds number and inevitable variations in leading-edge shapes, surface smoothness, and freestream turbulence levels. For the F-15, f_{Pk} also decreased with increasing angle of attack (as did the tail vibration frequency in the flight test), but in a complex manner. While this matching is a very encouraging finding, this does not tell us what particular length dimension is of physical significance, only that increasing the size of the model by a factor would reduce the frequency by the same factor. We used Strouhal number based on mean aerodynamic chord.

2.3 Observed Features

References 6-17 provide representative samples covering much of what is published on the dynamics of leading edge vortex flows and vortex breakdown. We will focus for now on the specific problem of tail vibration relevant to aircraft with moderately-swept wings. On such configurations, the narrow band phenomenon is observed even at angles of attack above the range where vortex core bursting is observed over the wings. An example is the F-15.

Sharp-Peaked Velocity Spectra

Ref. 6 describes wind tunnel tests on a 13% F-15 model using rigid tails, with hot-wire measurements, tuft tests, and smoke trail photos. The smoke tests attempted to determine a trajectory for the flow impinging at the top of the vertical tails and found that this passed above the "gun bumps" on the engine inlets. The hot-wire results showed sharp-peaked spectra near the rigid tails, just as we measured in Ref. 5. The value of $f_{Pk}L$ from these tests is seen on Fig. 3.

Broadband Pressure Spectra under Tail Boundary Layer

Triplett[7] reported surface pressure and accelerometer data on F-15 model tails in wind tunnel tests, using both rigid and elastically-scaled tails. The surface pressure fluctuations, measured with Kulite transducers on the tail surface, showed relatively broadband spectra for the rigid tails and of course sharp spectral peaks at the vibration frequency for the elastic tails. This appears to be one of the origins of the "broadband turbulence" hypothesis where the tail structure was thought to respond at its structural modes to a broadband forcing from the turbulent flow. Note that surface pressure transducers capture the pressure fluctuation beneath a turbulent boundary layer: the small-amplitude narrow-band velocity fluctuation may not show up in these data. Recently, Ashley et al.[15] have pursued active-control strategies to cancel vibrations of the F-15, regardless of precise details of the flow excitation.
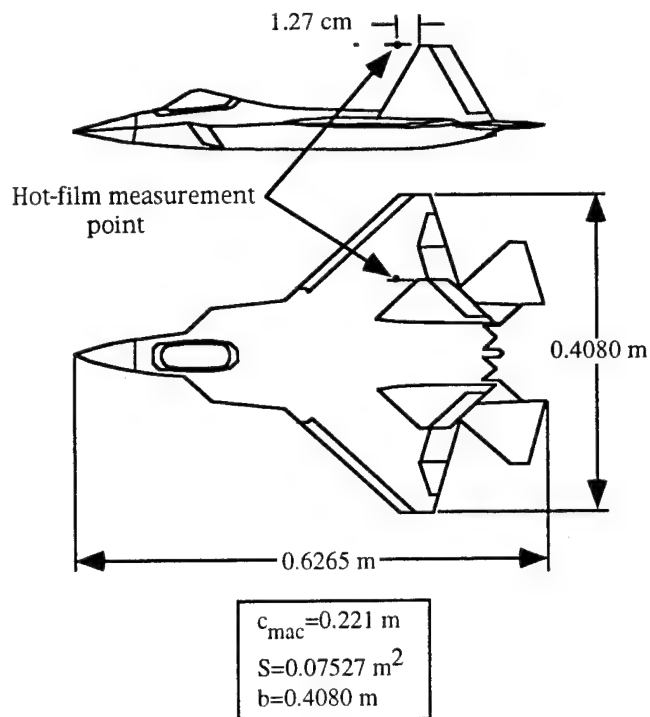
No Strong Vortex Cores over F-15

Ref. 16 confirmed our observation of Ref. 1 that the flow over an F-15 at $\alpha \geq 20$ deg. does not contain strong vortex cores whose "bursting" would explain the observed fluctuations. We note that our observations of the overall time-averaged F-15 flowfield were directly confirmed by the Navier-Stokes calculations of Ref. 4, as shown on Fig. 1.
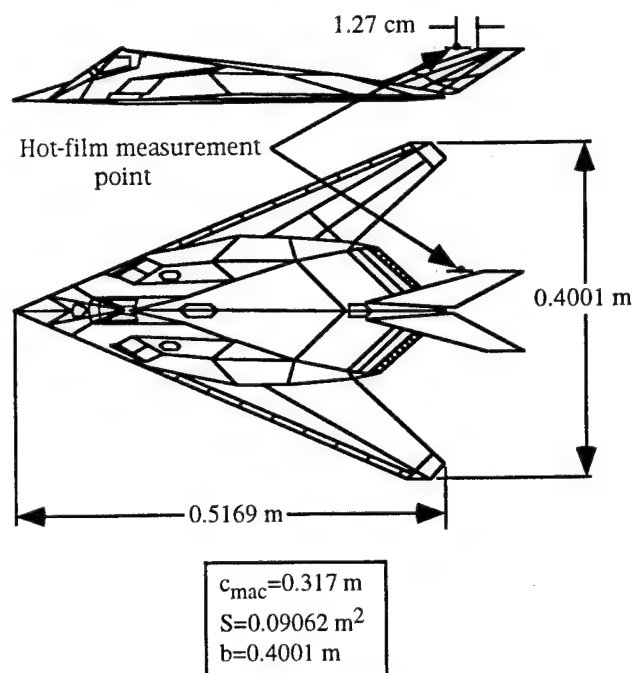
Quasiperiodic

The sharp-peaked spectra as shown in Fig. 2 indicate a periodic phenomenon with a very narrow band of frequency. Ref. 17 obtained similar results on a canard-wing fighter configuration with moderate sweep. The signal, however, exhibits considerable phase "jitter" and cycle-to-cycle variation in structure shape, as discussed later. While the phase is not as chaotic as in the case of natural instabilities of an unforced shear layer, it is far from being as regular as, for instance, a rotor flowfield.
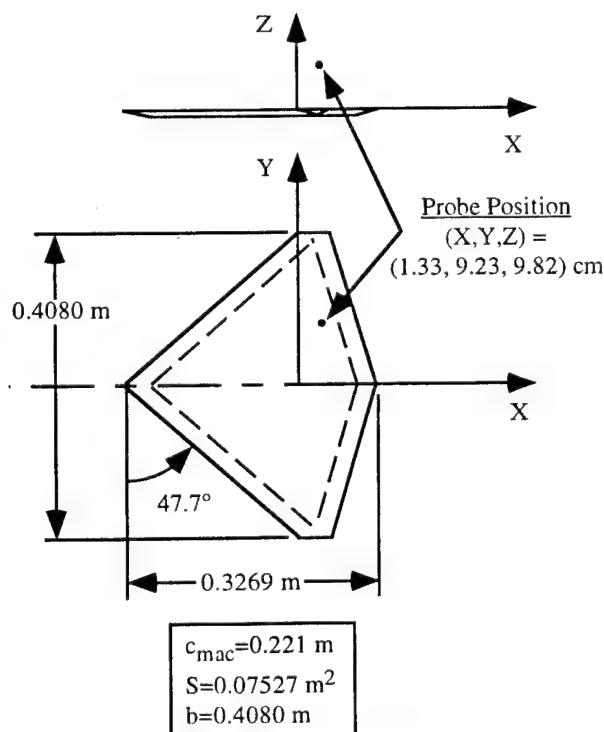
Seen on Many Configurations

We have measured such spectra over many configurations at angle of attack. These include 1/32 scale F-15s (with and without tails, engine through-flow, and inlet droop), above the burst-vortex (and above the tops of the tails) of a 1/32-scale F/A-18, an F-117, a generic double-swept delta wing/body of revolution model (Ref. 18), a YF-22, isolated wing planforms equivalent to most of those models, and a 59.3-deg. delta wing. In each case the measuring location was selected upstream of where the top of one of the tails would be located. In every case except the F-117 (whose geometry appears to generate several vortices), the f_{pk} vs. U_∞ line remained straight. Fig. 4 shows some of these data. Details are given in Ref. 19.
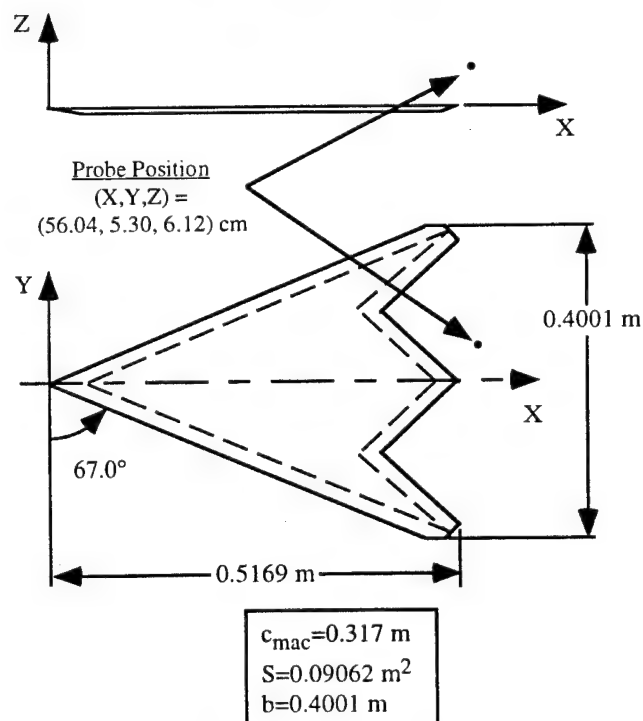
1.27 cm

Hot-film measurement point

0.4080 m

0.6265 m

$c_{mac}=0.221$ m
$S=0.07527$ m^2
$b=0.4080$ m

YF-22 1/32-scale model showing hot-film measuring position.

1.27 cm

Hot-film measurement point

0.4001 m

0.5169 m

$c_{mac}=0.317$ m
$S=0.09062$ m^2
$b=0.4001$ m

F-117 1/32-scale model showing hot-film measuring position.

Z

X

Y

Probe Position
$(X,Y,Z) =$
$(1.33, 9.23, 9.82)$ cm

0.4080 m

X

47.7°

0.3269 m

$c_{mac}=0.221$ m
$S=0.07527$ m^2
$b=0.4080$ m

YF-22 delta wing model showing hot-film measuring position.

Z

X

Probe Position
$(X,Y,Z) =$
$(56.04, 5.30, 6.12)$ cm

Y

0.4001 m

X

67.0°

0.5169 m

$c_{mac}=0.317$ m
$S=0.09062$ m^2
$b=0.4001$ m

F-117 delta wing model showing hot-film measuring position.

Figure 4(a): 1/32-scale models of the YF-22 and F-117 and the corresponding flat-plate wings tested.
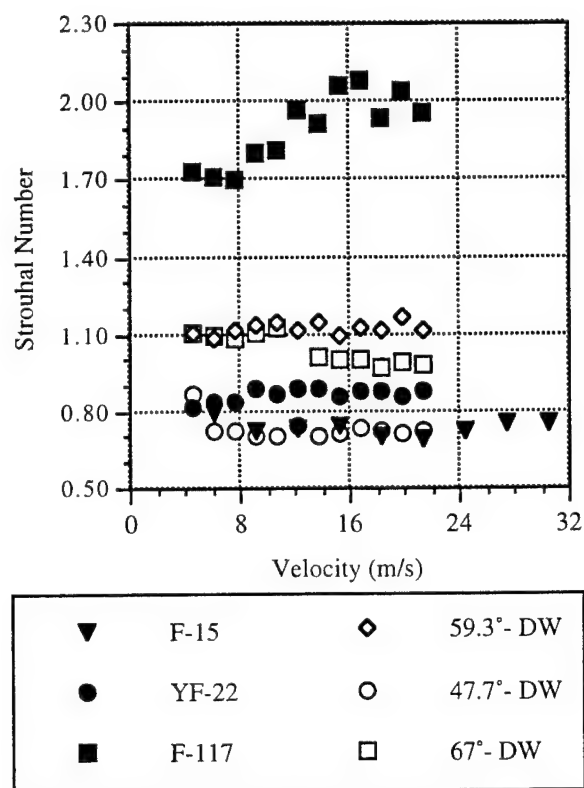
I-10

Figure 4(b): Strouhal number based on mean aerodynamic chord of the velocity fluctuations near the top of the vertical tail for various configurations and flat-plate wings, as a function of freestream velocity.
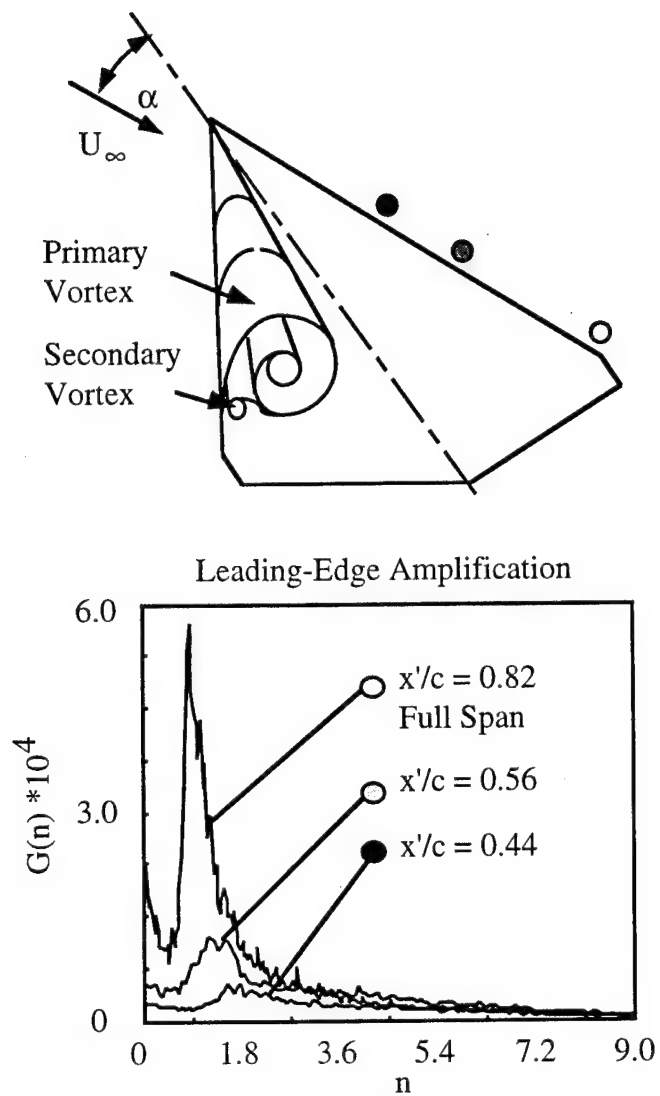
Figure 5: Spectral amplification and focusing along the leading edge of a
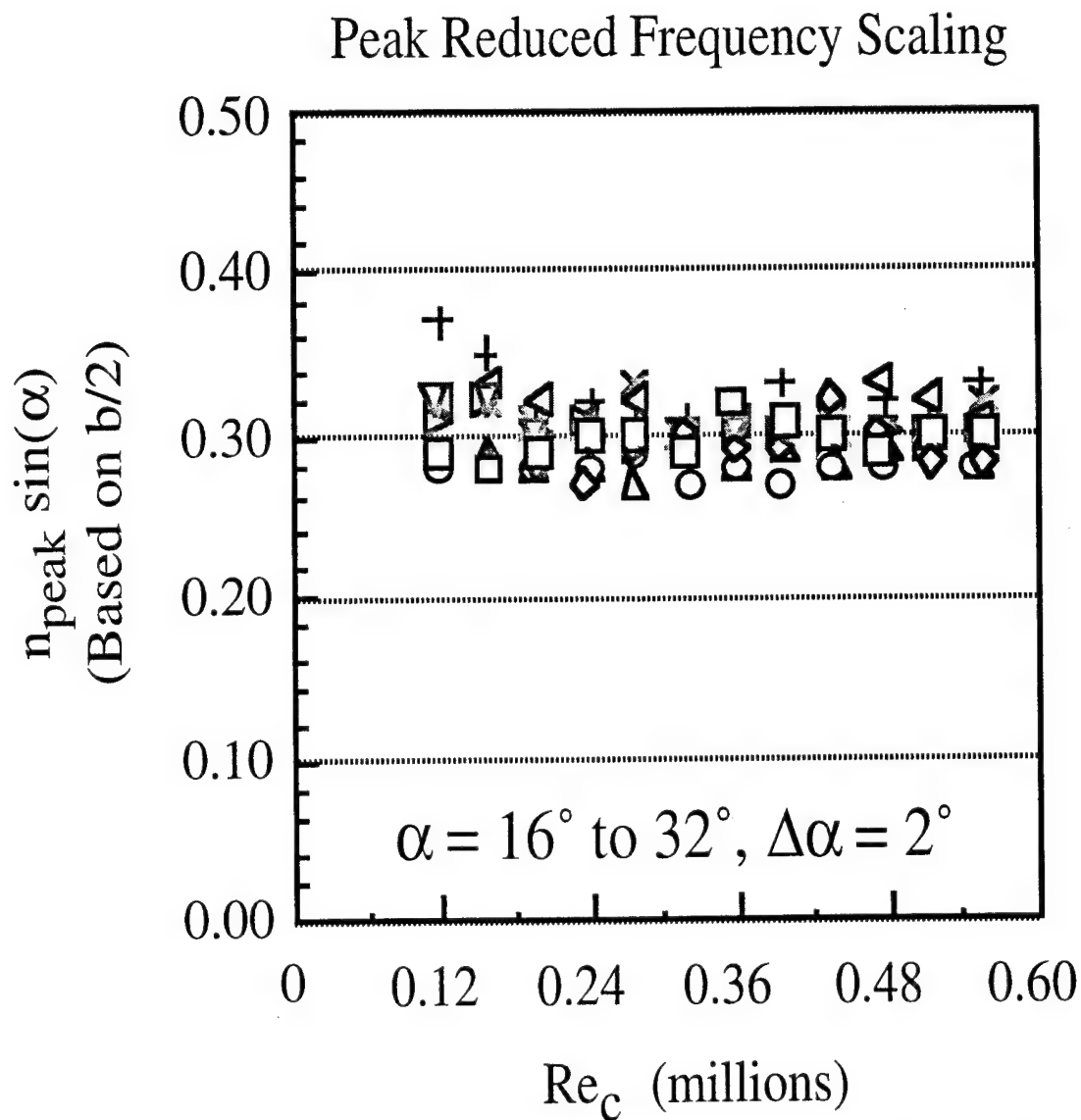59.3 cropped delta wing. From Ref. 1.

Peak Reduced Frequency Scaling

Figure 6: Peak frequency scaled by sin(α), vs. Reynolds number for a 59.3-deg. delta wing (Ref. 2).

Empirical Prediction: Full Configurations and Flat-plate Wings

The above tests showed that the presence of tails had nothing to do with the generation of the fluctuations. The effect of the fuselage and the rest of the configuration on the Strouhal number was noticeable but secondary, except for the F-117. The scale-model results of Ref. 19 provide a starting point for empirical prediction of possible driver frequencies for tail vibration; whether the results are as encouraging as those on the F-15, can only be determined from flight tests. We thus see that the basic phenomena can be seen on simple wing shapes: precise understanding of the frequency selection and amplification requires studies of "representative" configurations including the fuselage shape.

Spectral Characteristics and Scaling on a Delta Wing

Having determined that the basic phenomenon existed in the flow over an isolated, sharp-edged delta wing, we selected a 59.3-deg. delta wing to enable comparison with published data and with the extensive work elsewhere on vortex core bursting. This wing has beveled lower leading edges and trailing edges, and has been used in extensive measurements in two wind tunnels and is part of the generic wing-body model used in Ref. 18. Hubner and Komerath[20] plotted contours of f_{Pk} measured in a vertical cross-flow plane at the trailing edge at $\alpha = 25$ deg. The peak frequency is nearly constant over most of the plane, away from the vortex core. In the core region (post-burst), the frequency is lower, the spectrum is broader, and the amplitudes are high. Figs. 5 & 6 confirm the features seen on the F-15: the frequency decreases downstream along rays (inversely proportional to local span), the amplitude increases sharply, and the spectrum focuses into a narrow peak. Further downstream in the wake of the model, the peak frequency leveled off and the intensity decreased. Fig. 6 shows that the fully developed peak frequency scales with projected-chord for the isolated wing, as opposed to the full F-15 configuration, where Ref. 5 found a sharper variation of the peak frequency with varying α.

Coherence Tracking

Starting with two hot-film sensors at the trailing edge plane, we "walked" upstream along the path of highest coherence and intensity at the frequency f_{Pk}. As we moved upstream, f_{Pk} changed, increasing upstream as noted on Fig. 5. The trajectory is shown in Fig. 7, from Ref. 20. The structures responsible for these fluctuations appear to originate near the surface, around 1/3 chord from the apex for this case, and to take a helical trajectory around the periphery of the vortex. Thus it is not surprising that the smoke trajectory test of Ref. 5 showed the tail being hit by flow coming past the F-15 gun bump.

Top View:

Y, y'

1

8

X, x'
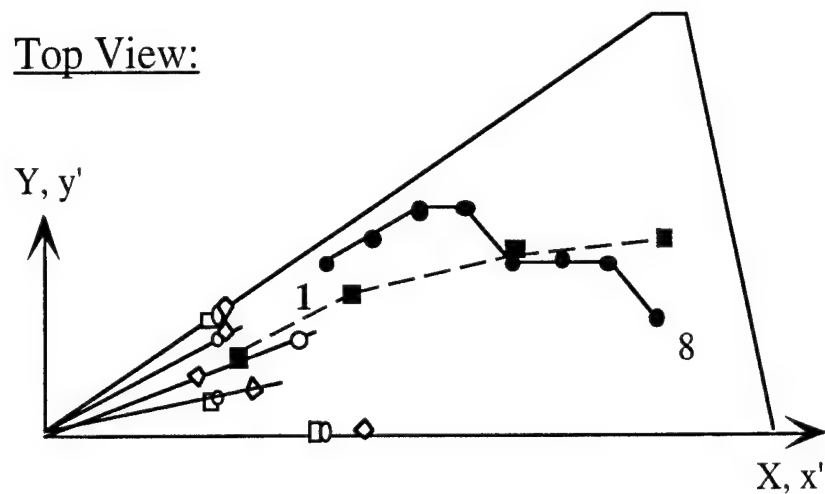
Legend:

● High Coherence/Intensity
  Trajectory Marking
■ Vortex Core
  Trajectory
□ Origin: $\theta = 4°$

○ Origin: $\theta = 8°$

◇ Origin: $\theta = 15°$

Side View:

Z   z'

X
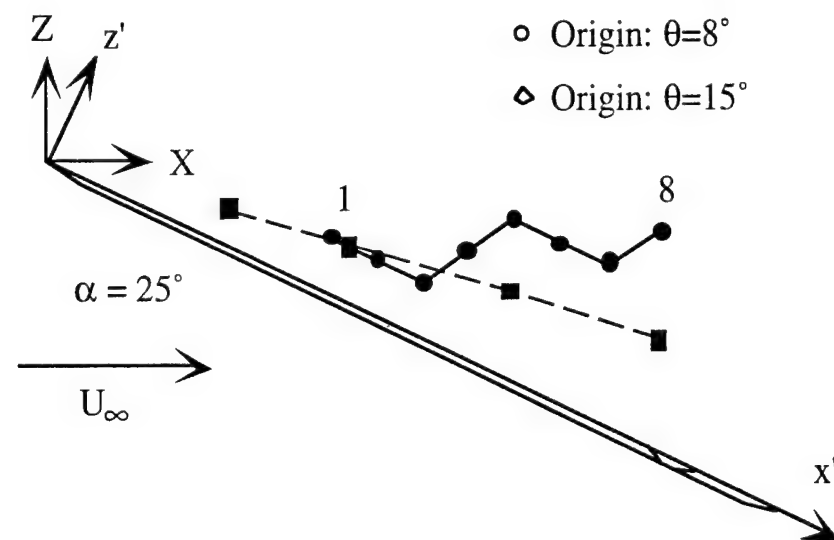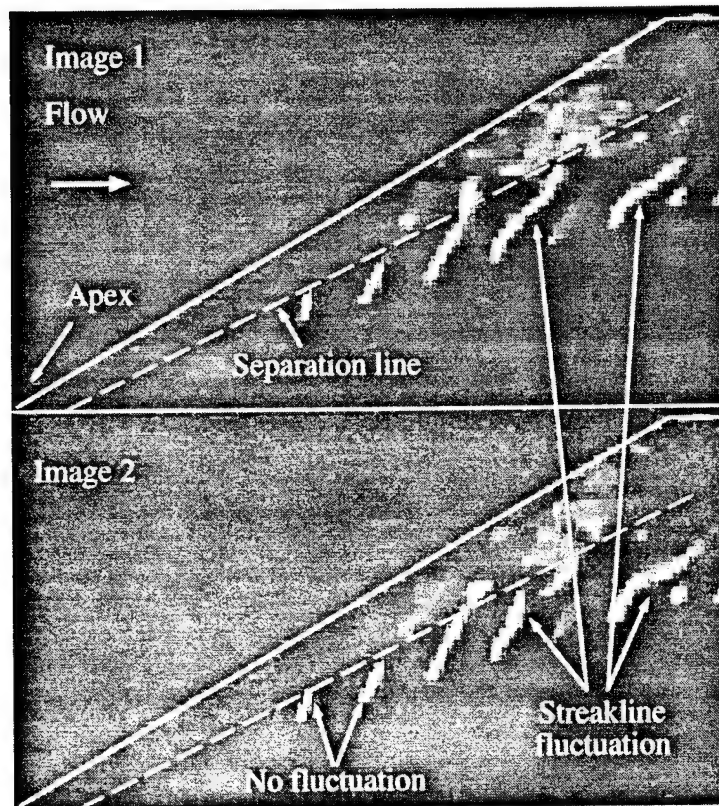
1   8

$\alpha = 25°$

U_∞

x'

Figure 7: Trajectory of high coherence and energy at the spectral peak frequency for a 59.3-degree delta wing.

Top View:
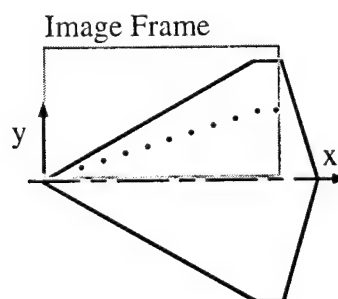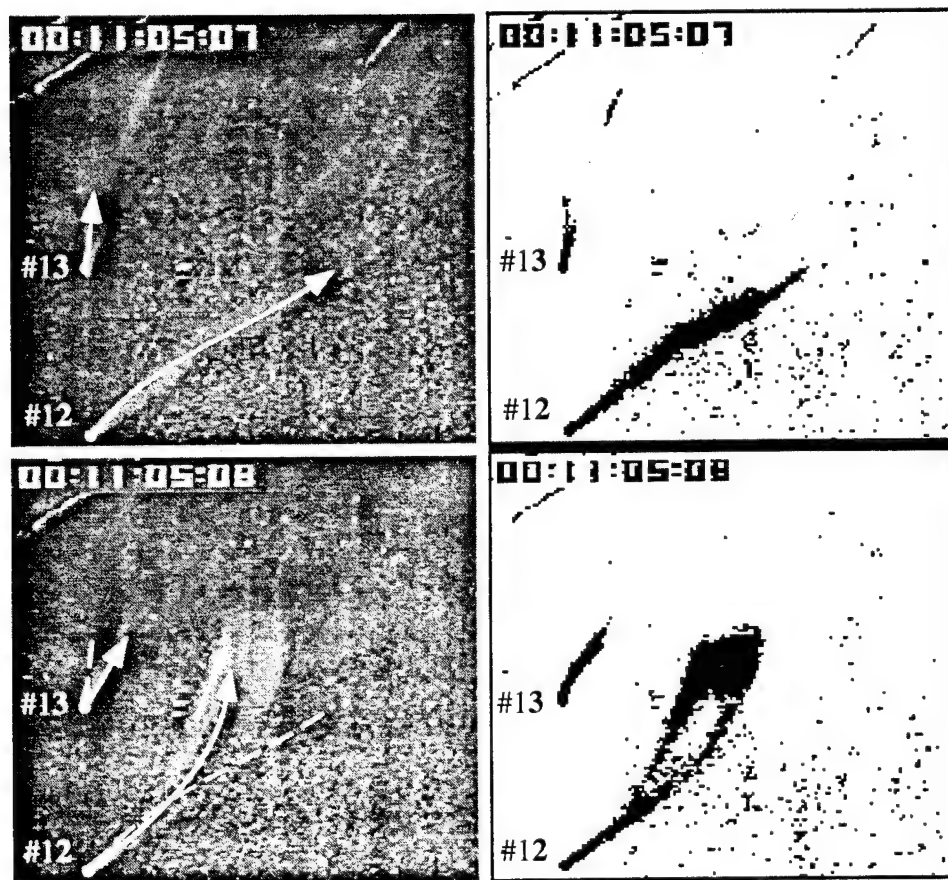
Figure 8(a). Visualization of multiple surface streaklines: $\alpha = 20°$, $U_\infty = 1.5$ m/s.

Video Image   Inverted Theshold Image
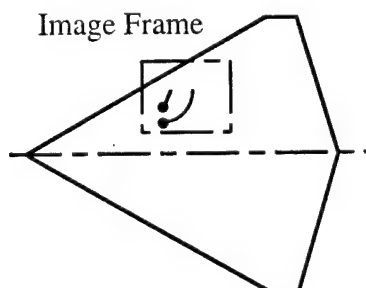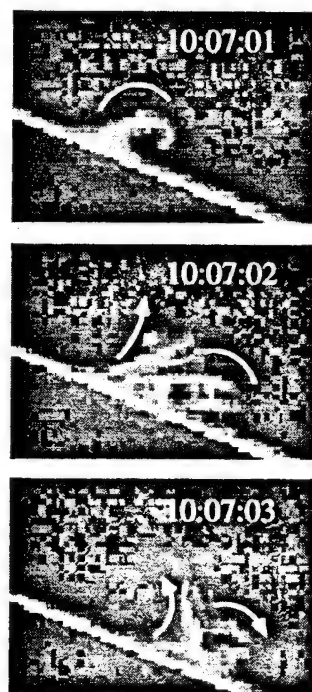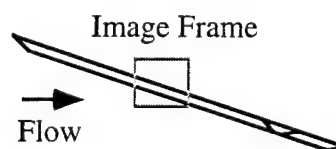
Top View:

Image Frame

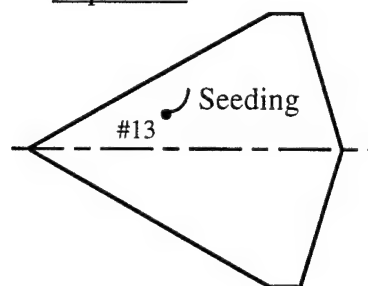Figure 8(b) Visualization of surface streaklines from ports #12 & # 13: $\alpha = 25°$, $U_\infty = 0.46$ m/s.

Figure 9. Visualization of streakline eruption: $\alpha = 20°$, $U_\infty = 1.5$ m/s.

Surface Streakline Fluctuations

Having established the results of Figs. 5-7, we concentrated attention at the surface. Smoke was entrained into the surface layer through small surface ports. A laser sheet parallel to the wing surface illuminated a 2 mm thick region above the surface. Fig. 8 shows the surface streaklines. They are oriented approximately spanwise (as is well known), but also show a periodic "waving". We counted the frequency of this waving, by manually checking the change in frame code of the video tape over several cycles of the waving. The tunnel speed and model size were chosen low enough to keep the frequency in the 10 Hz range, well below the 60 Hz framing rate of the camera. *The frequency fell on the* fp_k *vs.* U_∞ *straight line for this wing*, as first reported in Ref. 20. This was repeated, with more ports, and two different tunnel speeds. A hot-film spectrum acquired near one of the ports, at the higher speed, verified the video-counted frequency directly. We were seeing evidence of structures of the correct frequency, very near the surface. The amplitude of the waving increased downstream. Also, viewing the waving of streaklines from all ports together, it was evident that this was not a "stationary" phenomenon: the waving was sequential, clearly indicating that the structures were moving downstream.

Streakline Waving and Vortical Structures

Next, a chordwise vertical visualization plane cut across these streaklines. Fig. 9[21] shows vortical patterns of smoke, lifting off the surface layer and into the main vortex flow above. Again, these moved downstream. At the time, the sudden lifting was not understood: we were looking for a cross-flow shear layer roll-up. Our interpretation is also sketched in Fig. 9.

2.4 Tested Hypotheses

Over the years, we have tested many hypotheses about these fluctuations.
1. "Gun-bump" and "engine-inlet vortices" were ruled out: drooping the inlet, altering inlet flow (external acceleration, deceleration, and blocked) had no effect[4] on the spectra near the tails.
2. Removing the tails caused no change in the spectra measured upstream of the tail location.
3. In Ref. 6 we showed that a large vertical "splitter plate" along the spine of the F-15 model did not affect the spectra. This ruled out hypotheses about unsteady lateral coupling between the wing/forebody vortex systems.
4. Entrained vortices rotating around the primary vortex rotate at the wrong frequency. Forebody vortices entrained and rotating around the wing vortices might cause fluctuations at a fixed sensor. Some such cores are seen in videotapes from the generic wing-body model[18]. Tangential velocity data showed that these structures would pass the hot-film location at a completely wrong frequency.

5. Wing vortex shedding occurs only at a much higher angle of attack. What we see has nothing to do with large-scale shedding as seen by Redionitis et al.[22] at very high (>45 deg.) angles of attack: note that we measure a vortex velocity field which is steady in the mean.

6. The frequency of discrete vortical structures in the leading edge shear layer, attributed to Kelvin-Helmholtz instability, scales as the square root of the freestream velocity[23,24]. At freestream speeds higher than those used in water tunnels and flow visualization, the discrepancy between this frequency and the f_{pk} measured by hot-film sensors begins to glare. The experiments in Ref. 24 did not connect the low-speed "control" results and the higher-speed frequency measurements. This hypothesis appears to have been discarded (Ref. 22). Finally, using photography and direct frequency measurement, we have confirmed that the shear layer frequency is not in the range of interest.

7. The frequency of rotation of spiral breakdown matches the measured f_{pk}. However, spiral breakdown immediately leads to chaotic flow downstream. Thus, on wings where a strong core does exist in the region where these sharp-peaked spectra are measured, a "chicken-or-egg" question arises: Does spiral breakdown cause the surface fluctuations or vice versa? To answer this, consider a moderately-swept wing (the 45 deg. F-15 wing) at $\alpha > 20$ deg. Here an un-burst core cannot be detected; yet the fluctuations appear to originate near the surface, *and grow and focus downstream*, in an otherwise highly turbulent flowfield. Thus *the surface layer fluctuations are the more basic phenomenon*. Spiral core breakdown does not explain results on moderately swept wings.

8. "Helical mode hydrodynamic instability of the velocity profile in the core region of the post-breakdown vortex" has been cited by Gursul[25] as the complete mechanism of the periodic fluctuations. There are some aspects of the phenomenon which do correspond to helical modes of wave propagation, but this explanation is far from complete. Examination of the results in Ref. 25 shows that the helical mode explanation does not perform well for even the 70- and 75-degree swept wings, and does poorly for lower sweeps. Ref. 20 shows that the coherence of these fluctuations is actually quite low in the post-breakdown core flow, and the frequency is quite different from that measured in the outer annulus. This is clear evidence that the fluctuations do not originate in the post-breakdown core region. Also, as shown below, very small "fences" placed on the wing surface, far downstream of vortex breakdown, modify the entire fluctuation field very substantially. Finally, our LV measurements discussed below (where velocity components are measured without the directional ambiguity inherent to single-sensor hot-film anemometry) showed a 180-degree phase difference between measurement locations separated vertically, when the measured components were the axial and the vertical. This also argues against the "helical mode" explanation.

2.5 Surface Shear Hypotheses

Unsteady Secondary Separation due to Vortex/Surface Interaction

Visbal[14] has observed fluctuation of the secondary separation line in computations. We see this too, in visualization above the 59.3-deg. delta wing, though intermittently. Is this a cause, effect or something in between? The evidence to-date does not permit a clear answer.
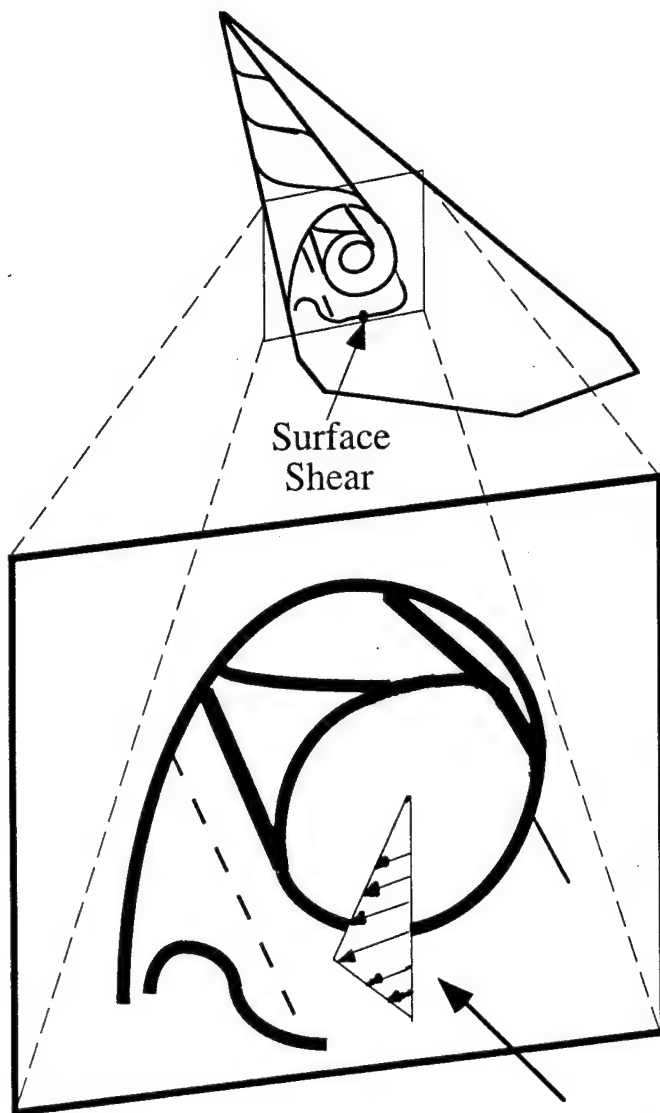
Centrifugal Instability

Rayleigh's second theorem on the instability of velocity profiles[26, 27] states that the profile is unstable if, anywhere in the flow,

$$\frac{d(rV)^2}{dr} < 0 \qquad (2)$$

where V is the tangential velocity and r is the radial distance from the center. The presence of axial velocity generally narrows down the range of this instability, as seen by many researchers. The occurrence of this condition at the surface under the primary vortex is sketched in Fig. 10. Deceleration at the surface must cause the tangential velocity profile of the vortex flow to drop sharply near the surface, leading to possible centrifugal instability of the flow. A counter-rotating pair of vortices must then be generated at the "preferred" frequency and spatial scale, lift off, and go around the periphery of the vortex. In the front parts of the wing, these structures may go around the vortex and interact again with the surface layer, focusing the roll-up into themselves and amplifying greatly. This phenomenon, given a velocity profile with the right unstable characteristics, is essentially independent of Reynolds number. In a helical flow, the measured velocity disturbance at a fixed point due to the passage of these counter-rotating structures will be merely a periodic velocity fluctuation. We proceed to detail recent evidence of such structures, after considering the obvious question: Why was this not seen before?

Re-examination of the literature on leading edge vortices encourages this model. Ludwieg[8] showed instability of vortex flows in annular regions bounded by solid walls, and predicted instability when streamline inclinations reached about 42 degrees (see Fig. 8 for our streakline orientations). He proposed that this type of three dimensional disturbance causes the breakdown of free vortices over delta wings. Unfortunately, research since then appears to have focused on the core of the vortex. Ludwieg's approach was rejected by many subsequent reseachers because the solid wall boundary condition was considered inapplicable to the core flow instability problem[10]. In addition, stability of the core flow was shown when there was a substantial axial velocity in the core. Again, note that our interest is not in the development of instability of a vortex core flow: it is in the development of organized structures around the

Surface
Shear

*Region of postulated centrifugal
instability: Tangential velocity profile
decays outward faster than 1/r.*

Expanded view of flow cross-section

Figure 10: Decelerated flow region between the surface and the vortex core,
susceptible to centrifugal instability and the generation of counter-rotating
spanwise structures.

periphery of a turbulent vortex flow where the core may have already become chaotic, and the axial velocity in the core may be insignificant. In fact, in the post-burst flowfield, the cross-sectional velocity profile of the vortex is known to be essentially a solid body rotation. Here, Ludwieg's analysis should be re-examined. Leibovich[10,11] emphasizes that the role of asymmetric and 3-D disturbances is simply not known, and in later publications considers both symmetric and asymmetric disturbances to a cylindrical vortex core flow. Stability criteria developed for inviscid columnar vortices, based on the axial and azimuthal gradients, are sufficient to explain the formation of spiral disturbances similar to Ludwieg's. Disturbances of this nature could explain the observed focusing of flow energy away from the core. Escudier[9] shows why much of the research on vortex stability would not have found a centrifugal instability mechanism: it generally assumed an inviscid, steady laminar flow around the core, and thereby would not have the shear at the wall which produces the unstable velocity profile in this case. The assumption of inviscid flow has been justified on the grounds that vortex breakdown phenomena appear not to depend on Reynolds number except for the core velocity profile. Our quasiperiodic disturbances also are independent of Reynolds number, but shear at the wall is necessary to set up the unstable region. The precise size of this region appears not to play a role.

Quantitative Evidence of Counter-Rotating Structures

In Ref. 28 we verified that spectra obtained with a fiber-optic laser velocimeter (LV) are the same as those obtained with a surface hot-film sensor immediately upstream of the LV measurement location. We obtained ensemble-averaged traces of velocity fluctuations, measured from the LV data phase-synchronized with a trigger generated from the hot-film signal. The amplitude of the phase-locked variation was only about 20% of that measured from the spectral energy at this frequency, primarily because the later portions of the cycle were smeared considerably: this is because the phenomenon is "quasiperiodic", not quite the same in phase or frequency from cycle to cycle. However, we used the data to generate a map of the periodic fluctuations in a vertical plane as shown in Figs. 11 a and b. *They show quantitative evidence of counter-rotating, periodic structure in this section.*, strengthening the visual evidence of Fig. 9. It is emphasized that these data underestimate the strength of these structures because of the deviations from periodicity. The size of these structures is bigger than the measuring grid.

Spectra Are Sensitive to Surface Disturbances

The last piece of evidence for the surface-layer hypothesis is that we are able to modify the spectra without significantly modifying the overall flowfield or the lift and drag, by placing small (height on the order of the boundary layer thickness) fences on the surface at different orientations. This is shown in Fig. 12 along with various fence orientations. Ref. 5 also reports
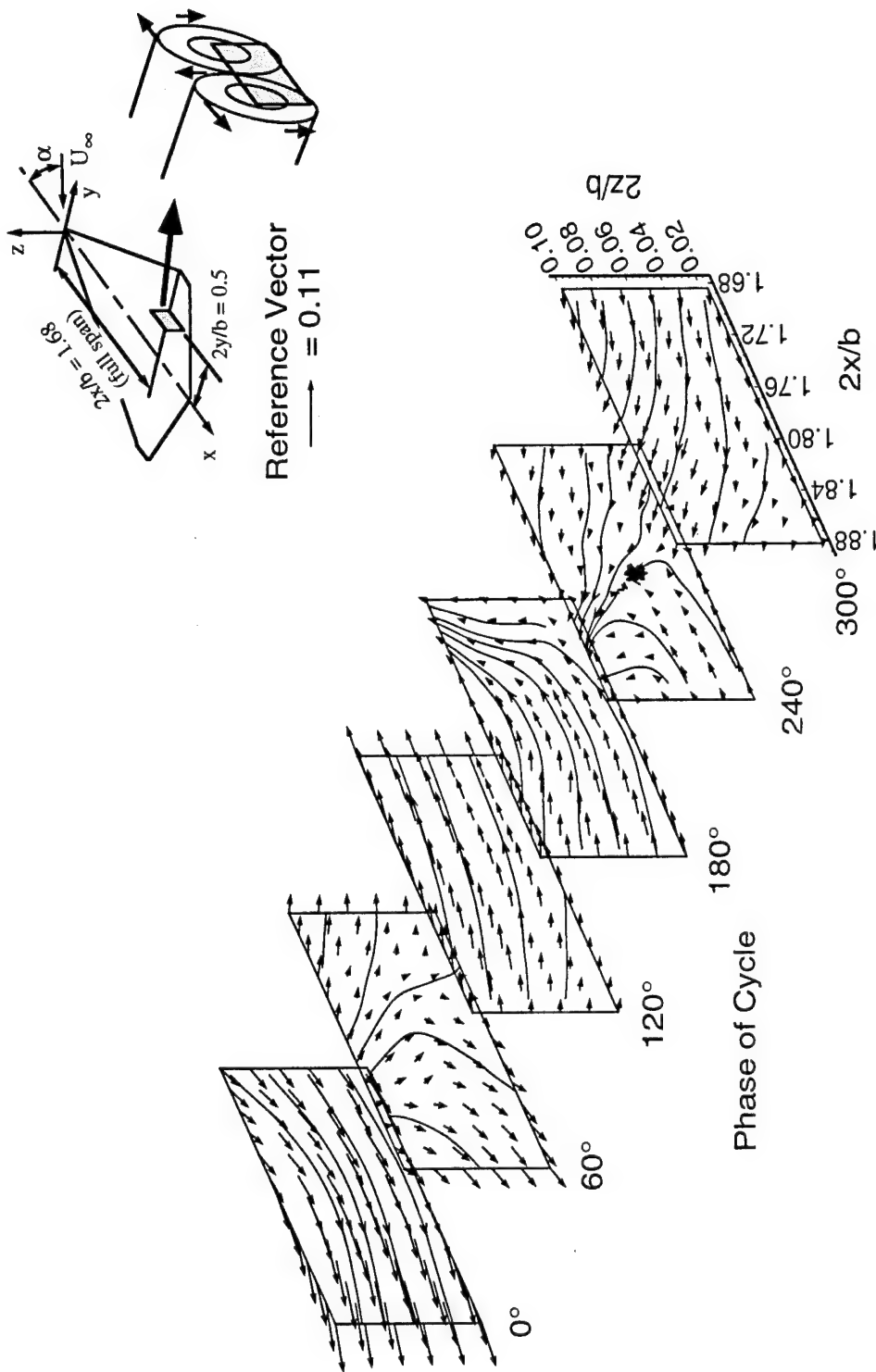
Figure 11a Phase-resolved, fluctuating velocity vectors along the inner measurement plane: $\alpha = 25°$, $2y/b = 0.50$.
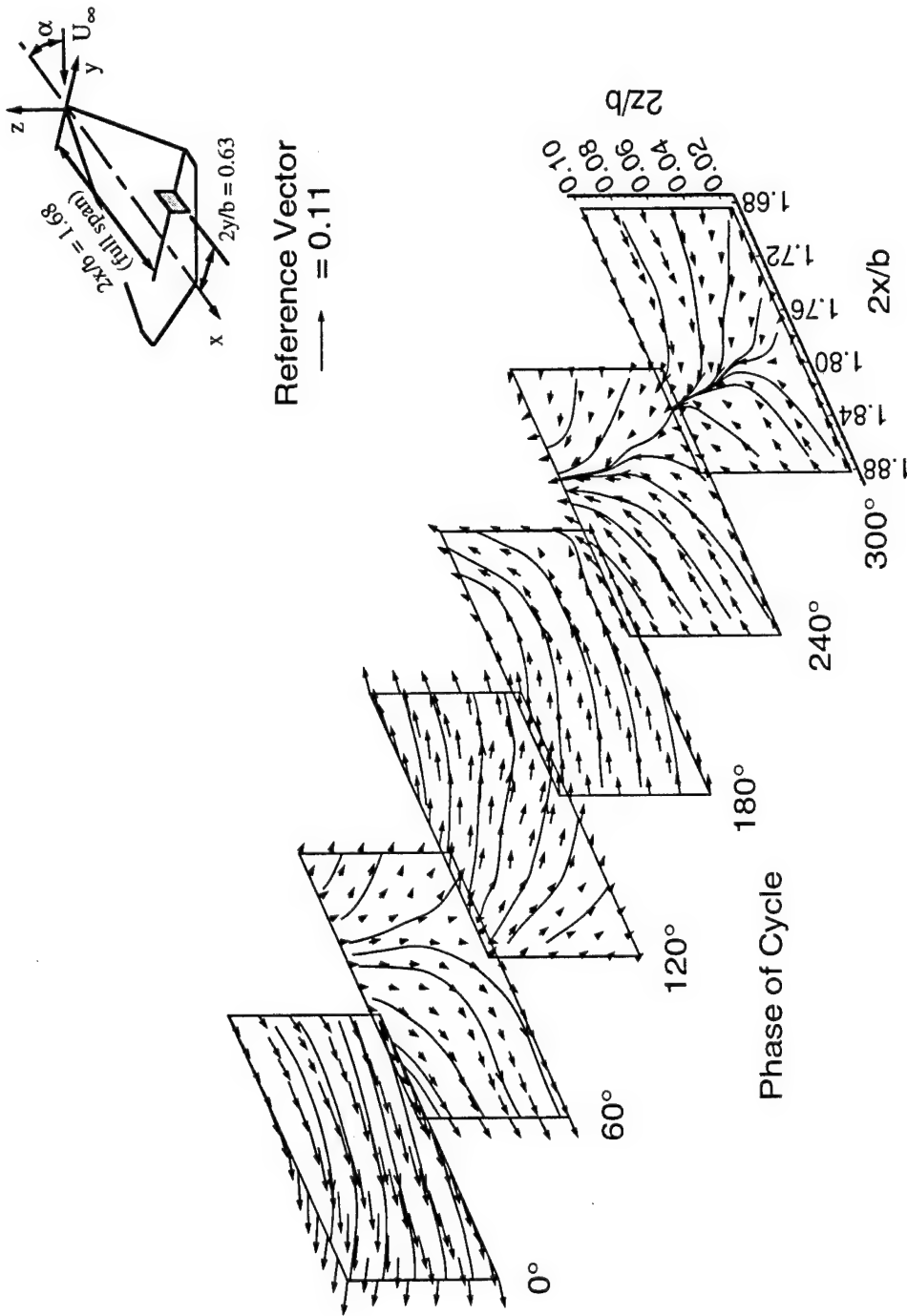
Figure 11b Phase-resolved, fluctuating velocity vectors along the outer measurement plane: $\alpha = 25°$, $2y/b = 0.63$.

surface modifications using inboard fences, aligned with the freestream direction and much larger than the boundary layer: these produced roughly a 50% attenuation of tail tip pod accelerations on the F-15. Here the fences used are extremely small in comparison. Modified spectra at a single measurement point are shown in Fig.12(b). An obvious question here is whether the attenuation at one location implies merely a shift in the vortex structure. This was answered in two ways. First, the lift, drag and pitching moment characteristics of the wings were measured with and without the surface modifications. The 3 types of fences shown had no measurable effect on the aerodynamic characteristics. When the same fence rods were placed along and under the leading edge, there was a substantial modification of the characteristics; hence these were not studied further. Secondly, surveys were made of the spectra in a cross-flow plane at the wing trailing edge with a hot-film sensor. The measurement plane is shown in Fig. 13(a), and contours of the intensity ratio in dB (defined as $10Log_{10}$(modified intensity /baseline value))were plotted. Attenuation of upto -3dB dB is shown over a large region using the fences of Type B orientation. On the other hand, orientation of Type C, placed further inboard, at the same angle of attack of 18 degrees, resulted in amplification over a large portion. At a = 25 deg., both types B and C resulted in attenuation of upto 3dB. Type D fences generally amplified the spectra. These results indicate several points. Firstly, the spectral intensities up near the vertical tail top location are substantially modified, with no other discernible change to the flow, by these mini-fences placed far downstream. This tends to confirm that the fluctuations do not originate in the core region, but at the surface. Secondly, the amplification of the fluctuations by Type D fences (which are aligned approximately parallel to the surface streaklines and hence will not interfere with the development of the counter-rotating structures) strengthens the centrifual-instability argument and destroys the "helical mode" argument.

Görtler vortices or Cross-Flow Shear Layer Instability?

The formation of asymmetric structures in an environment with mean streamline curvature indicates an interaction between the centrifugal forces and the radial pressure gradient of the primary vortex. Schlichting[26] and the review by Saric[27] indicate that counter-rotating vortex pairs of this type can properly be called Görtler vortices. The upflow between these structures, cited as evidence of Görtler vortices in previous experiments cited in Ref. 27 is also seen in the LV data and the behavior of the surface smoke streaklines. On the other hand, the near-wall region has a severe cross-flow shear layer, and instability of this shear layer may also play a role. It is easy to conceptualize such a flow tending to produce roll-up, but not counter-rotating structures. Research on cross-flow instabilities on swept wings has focused in the area of boundary layer transition and appears not to have reached the high-angle-of-attack case of interest here.

Radial Fences:

β = 22.5°
Type B

β = 18°
Type C

Lateral Fences:

Type D
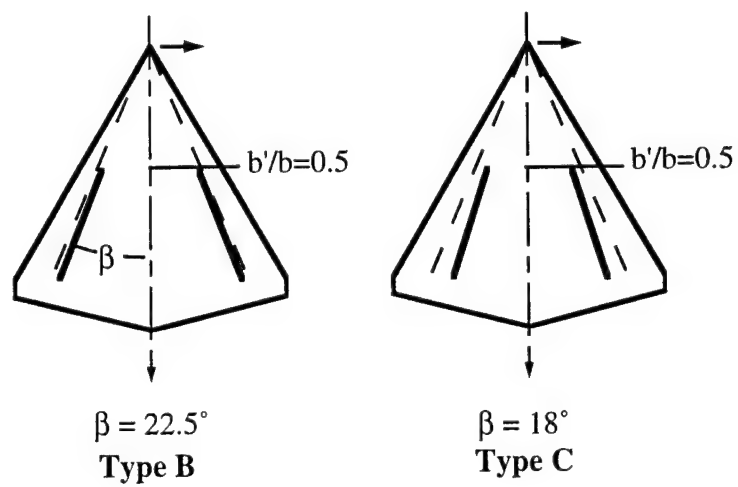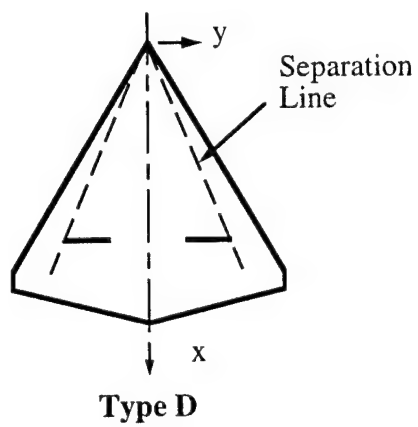
Figure 12(a): Diagram of surface fence orientations.
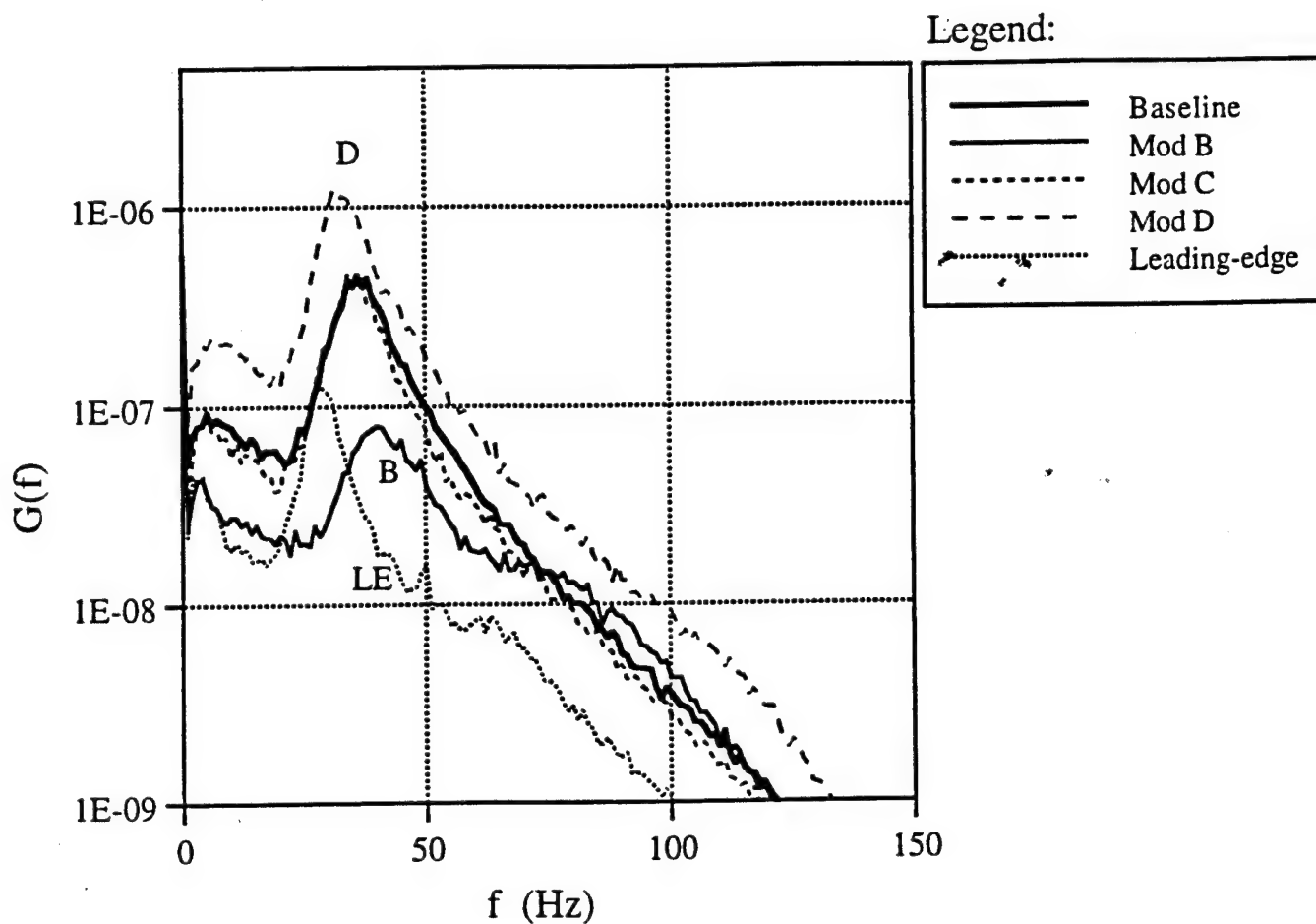
Figure 12b: Single-point velocity spectra measured near the approximate
vertical tail location over a 59.3-deg. cropped delta wing, with and without
surface fences of various orientations.
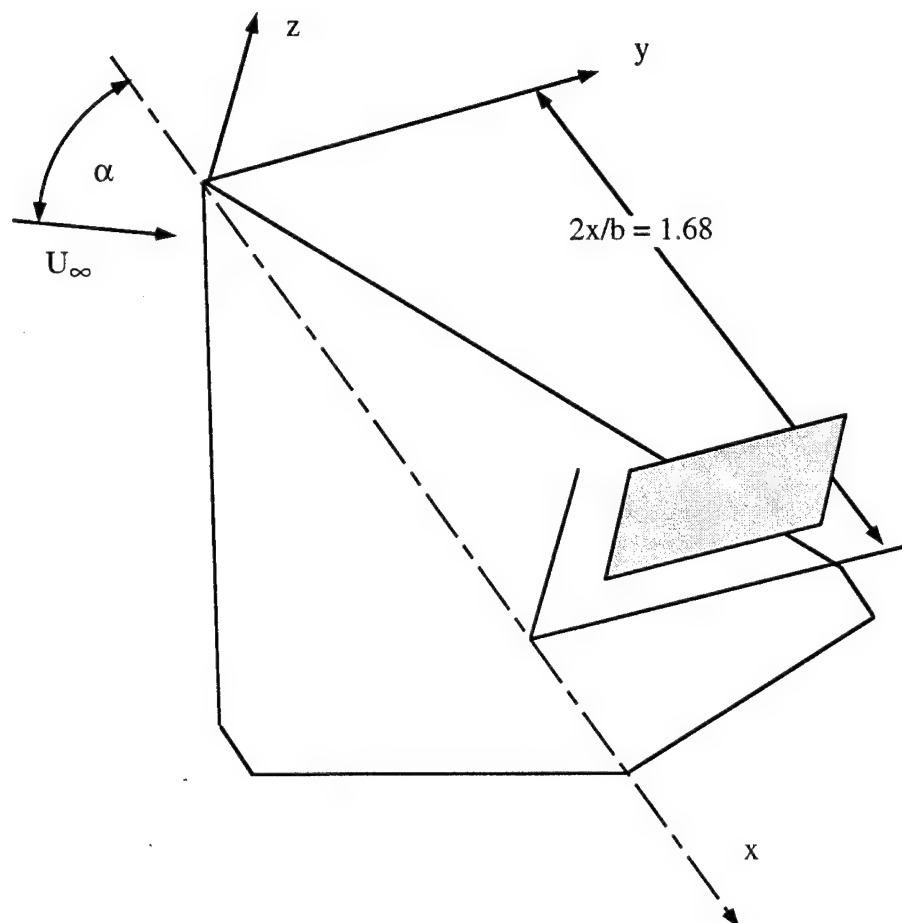
Figure 13(a): Measurement plane for hot-film survey of spectral modification

(a)

(b)
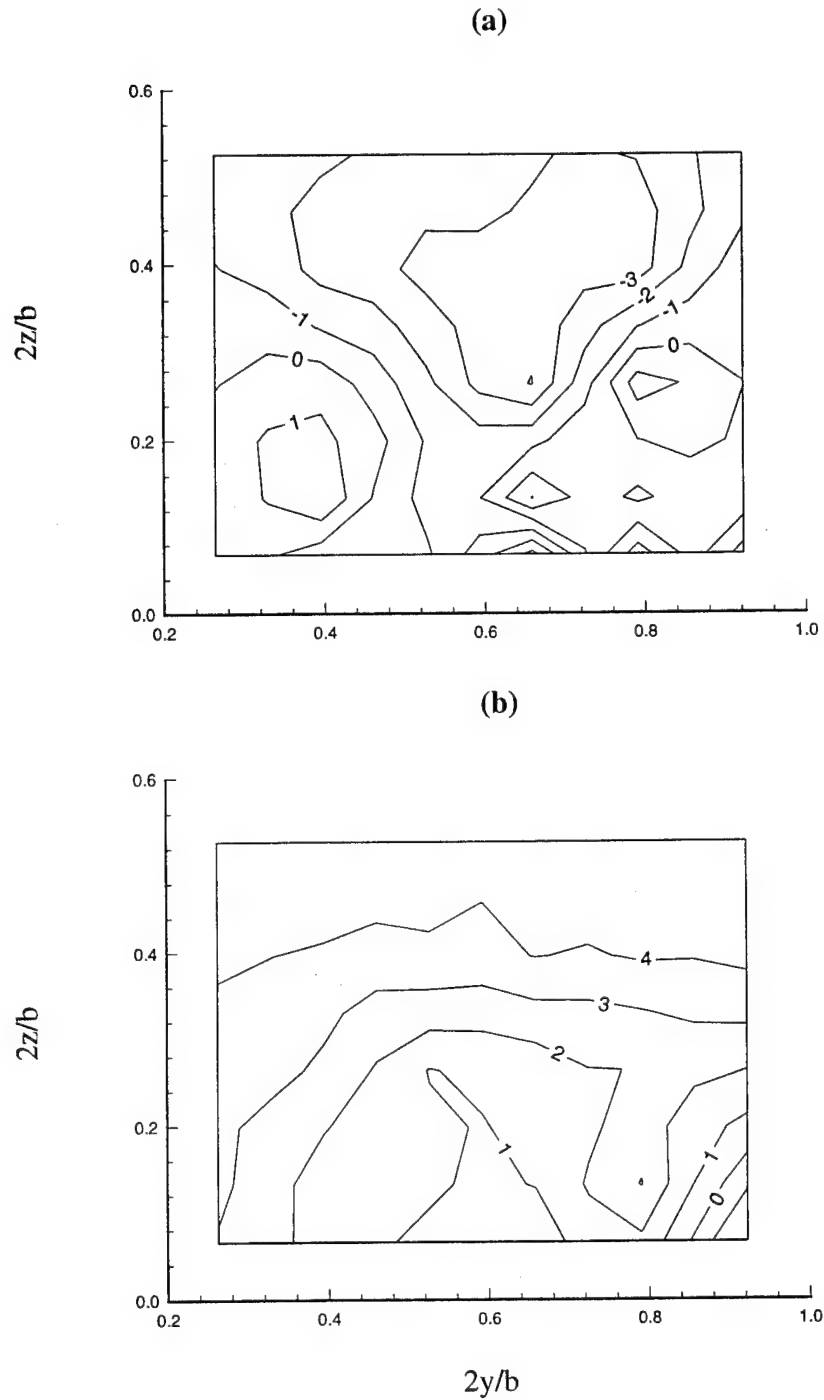
Figure 13(b): Peak intensity comparison contours of flow fluctuations:
(A) modification type B and (B) modification type C. ($\alpha = 18°$).

In concluding this section, we note strongly that the phenomena originate in the region between the primary vortex core and the wall. The right answer is probably a combination of centrifugal instability, cross-flow shear instability, unsteady boundary layer separation due to the secondary vortex, and perhaps other as-yet-unseen mechanisms.

2.6 Summary Of Present Knowledge

It is clear that nearly-periodic drivers exist in nominally steady vortex flows for a wide range of conditions. Empirical prediction of the possible driver frequencies for a given configuration can be obtained by measuring velocity spectra over scale models in low-speed wind tunnels at varying speeds and angles of attack. Where structural modes coincide with the driver frequency, vibrations may be expected. Critical vibration conditions will depend on the structural dynamics. The Strouhal number of velocity fluctuations on scale models matches that of tail vibration in flight test on the F-15; however, this is just one datum, and more data are needed from flight tests on other configurations to verify that such an approach will work for other configurations. Success with passive control techniques is encouraging, and indicates that first-principles based prediction and suppression are possible. Success would lead to a broad-ranging prediction capability on a very important problem, and guide flow modification techniques to prevent the amplification of these fluctuations. Combined with the empirical findings, this can also lead rapidly to a design-stage capability to avert tail buffeting problems.

There are some clear differences between the violent fin buffeting encountered in burst-vortex flows, and the lower-amplitude periodic driving in the F-15 flows, as seen here. The latter phenomenon can drive insidious fatigue cracking over hours of operation at high angles of attack. This can be a serious problem as aircraft age, and newer engines and tactics require pilots to spend a longer portion of their flight hours practicing maneuvers involving high-α operation.

To achieve first-principles-based prediction, highly-resolved computations are required. Identification of the crucial phenomena is essential to this effort. After trying out many hypotheses, we see that the basic phenomenon is one which can be simulated using simple configurations, though precise prediction of frequencies does require inclusion of the full configuration. The phenomenon exists in every swept-wing vortex flow studied to-date, for angles of attack ranging from 15 to 40 degrees depending on the geometry. Our present understanding leads us to focus on flow structures originating in the surface shear layer. This is strenghtened by the observations of Ref. 13 where vortex-surface interactions are seen to cause fluctuations of the leading edge shear layer. The flow visualization and the velocity data synchronized with surface hot-films provides strong support for the argument that counter-

rotating vortical structures exist under the primary vortex core, and that these amplify and convect downstream, causing nearly-periodic velocity fluctuations everywhere in the vortex flow. It is argued that these structures correspond to expectations based on the centrifugal instability of the primary vortex flow as it is decelerated by wing surface shear. This also explains insensitivity of the Strouhal number to Reynolds number. The success in modifying the spectra without modifying the lift characteristics further supports the surface-origin hypothesis. The basic issue of secondary separation vs. centrifugal instability or other mechanisms remains to be resolved.

Measurement Uncertainty

As with all experimental results, measurement uncertainty must be quantified. The freestream velocity of the tunnel is accurate to within 1%: this is a major uncertainty for such a quantity, but its frequency content is extremely low; far below 0.1 Hz, which is the high-pass filter cut-off for fluctuating data. The spectra presented here were each obtained by ensemble-averaging 100 sample blocks of data. The analog-digital converters used in every case, whether with hot-film or LV data had a 12-bit mantissa and 4-bit exponent, with the signal level optimized to use the full scale in each case using amplifiers and on-line monitoring. The frequency response of the instrumentation exceeded the highest frequency of interest by at least a factor of 3 (the worst case was where streakline fluctuation frequencies of up to 10 Hz were counted using a 60-frame-per-second video system. Spatial dimensions are measured with accuracies of 0.25 mm for spans and chords and 0.25 deg. for angles; probe positioning accuracies are nominally 25 μm, but the measurement uncertainty of 0.25 mm controls this. The worst-case uncertainty is in the acquisition of phase-resolved LV data; deviations from periodicity of the trigger signal cause underestimation of the ensemble-averaged data by up to a factor of 5. In this case, improved measurements would clarify the phenomena which we have identified.

2.9 References

1. Hubner, J.P., *"An Investigation of Quasiperiodic Structures in the Vortical Flow Over Delta Wing Configurations"*. PhD Thesis, School of Aerospace Engineering, Georgia Institute of Technology, August 1995.

2. Magill, J.C., Komerath, N.M., *"Wind-Driven Dynamic Manipulator for a Wind Tunnel"*. U.S. Patent 5,345,818, September 1994.

3. Komerath, N. M., Liou, S-G., Schwartz, R. J., Kim, J-M., "The Flowfield of a Twin-Tailed Aircraft at Angle of Attack. Part I: Spatial Characteristics," *J. Aircraft*, Vol. 29, No. 3, 1992, pp. 413-420.

4. Kwon, O. J., and Sankar, N. L., "Viscous Flow Simulation a Fighter Aircraft," *J. Aircraft*, 1992, pp. 886-891.

5. Komerath, N. M., Schwartz, R. J., Kim, J-M., "Flow Over a Twin-Tailed Aircraft at Angle of Attack, Part II: Temporal Characteristics," *J. Aircraft*, Vol. 29, No. 4, 1992, pp. 553-558.

6. Colvin, B. J., Mullans, R. E., Paul, R. J., and Roos, H. N., "F-15 Vertical Tail Vibration Investigations," MDC Report No. A6114, September 1979.

7. Triplett, W. E., "Pressure Measurements on Twin Vertical Tails in Buffeting Flow," *J. Aircraft*, Vol. 20, No. 11, 1983, pp. 920-925.

8. Ludwieg, H., "An Explanation of the Instability of the Free Vortex Cores Occurring Over Delta Wings With Raised Edges," Report of the Aerodynamic Test Institute, Gottingen, 1961. Translated by Leo Kramer Associates, NASA TM-75861, September 1980.

9. Escudier, M., "Vortex Breakdown: Observations and Explanations," *Progress in Aeronautical Sciences*, Vol 25, 1988, pp. 189-229.

10. Leibovich, S., "The Structure of Vortex Breakdown," *Annual Review of Fluid Mechanics*, Vol. 10, 1978, pp. 221-246.

11. Leibovich, S., and Stewartson, K., "A Sufficient Condition for the Stability of Columnar Vortices," *J. of Fluid Mechanics*, Vol. 126, 1983, pp. 335-356.

12. Lee, M., and Ho, C-H., "Vortex Dynamics of Delta Wings," *Frontiers in Experimental Fluid Dynamics, Lecture Notes in Engineering*, Springer-Verlag, Vol. 46, 1989, pp. 365-427.

13. Lee, B. H. K., Brown, D., Zgela, M., and Poirell, D., "Wind Tunnel Investigations and Flight Test of Tail Buffet on CF/A-18 Aircraft," *Aircraft Dynamic Loads Due to Flow Separation*, AGARD-CP-483, 1990, p. 1-1 - 1-26.

14. Visbal, M. R., "Computational and Physical Aspects of Vortex Breakdown on Delta Wings," AIAA 95-0585, Jan. 1995.

15. Ashley, H., Rock, S. M., Chaney, K., and Eggers Jr., A. J., "Active Control for Fin Buffet Alleviation," WPAFB, WL-TR-93-3099, 1993.

16. LeMay, S. P., and Lovato, J. A., "Experimental Investigation of the Vortex-Vertical Tail Interaction on an F-15," AIAA 94-0700, Jan. 1994.

17. Breitsamter, C., and Laschka, B., "Turbulent Flow Structure Associated with Vortex-Induced Fin Buffeting," *J. of Aircraft*, Vol. 31, No. 4, 1994, pp. 773-781.

18. Komerath, N. M., Liou, S-G., DeBry, B., Caplin, J., Lenakos, J., "Measurements of the Unsteady Vortex Flow Over a Wing-Body at Angle of Attack," AIAA 92-2729, June 1992.

19. Klein, M., Hubner, J. P., and Komerath, N. M., "Spectral Measurements in Vortex Flow over Swept-Winged Configurations at High Angle-of-Attack," AIAA 94-1804, June 1994.

20. Hubner, J. P., and Komerath, N. M., "Spectral Mapping of Quasiperiodic Structures in a Vortex Flow," *J. of Aircraft*, Vol. 32, No. 3, 1995, pp. 493-500.

21. Hubner, J. P., and Komerath, N. M., "Visualization of Quasiperiodic Structures in a Vortex Flow," AIAA 94-0624, Jan. 1994.

22. Redionitis, O. K., Stapountzis, H., and Telionis, D., "Periodic Vortex Shedding Over Delta Wings, *AIAA J.*, Vol. 31, No. 9, 1993, pp. 1555-1562.

23. Gad-el-Hak, M., and Blackwelder, R. F., "The Discrete Vortices from a Delta Wing," *AIAA J.*, Vol. 23, No. 6, 1985, pp. 961-962.

24. Gad-el-Hak, M. and Blackwelder, R. F., "Control of Discrete Vortices from a Delta Wing," *AIAA J.*, Vol. 25, No. 8, 1987, pp. 1042-1049.

25. Gursul, I., "Unsteady Flow Phenomena over Delta Wings at High Angle of Attack". AIAA Journal, Vol. 32, No. 2, February 1994, p. 225-231.

26. Schlichting, H., *Boundary Layer Theory*, 7th Ed., McGraw-Hill, 1979, pp. 525-535

27. Saric, W., "Görtler Vortices," *Annual Review of Fluid Mechanics*, 1994, pp. 379-409.

28. Hubner, J. P., and Komerath, N. M., "Modification of Spectral Characteristics in a Vortex Flow Field," AIAA 95-1795, June 1995.

CAS

Consulting Aviation Services

1712 Victoria Way
Kennesaw, GA 30144

Report No. CAS-001

Version 1.3 of the High Angle of Attack Stability and Control, Preliminary Design Code

with Vortex Breakdown and Buffet Analysis

June 1995

Final Report for Part II of the Georgia Institute of Technology, AFOSR Contract: "Quasi-Periodicity in Vortex Flows." Conducted under Georgia Institute of Technology subcontract No. E-16-M65-S1

by Charles J. Dixon

Summary

The High Angle of Attack Stability and Control, HASC, computer code developed for the Air Force Wright Laboratory in 1992 has been significantly improved. These improvements are discussed and typical results given. The effect of camber or edge bevels on vortex loads and breakdown is accurately predicted. Experimental investigations of the vortex characteristics have improved the understanding of the vortex breakdown process. This knowledge has been incorporated in the HASC code. Effects of multiple vortices on vortex breakdown and the final vortex-burst analysis are significantly improved. It is shown that prediction of the vortex core size after the vortex becomes turbulent (vortex core spirals) is accurate. This turbulent vortex diameter can be used as the length scale in the reduced frequency of the quasi-periodic vortex buffet. Setting this reduced frequency to a value of 0.5 allows prediction of the frequency. The Appendix updates and clarifies some of the run techniques for version 1.3 of the HASC code.

1.0 Introduction

In 1992 the initial development of a preliminary-design high-angle-of-attack computer code was completed by the Lockheed Aeronautical Systems Company for the Air Force Wright Laboratory. The final report[1] was completed in October 1992. The code is called HASC for "High Angle of Attack Stability and Control." Although the code is called High Angle of Attack, it predicts the characteristics of the leading-edge free vortices including breakdown at what ever the angle of attack that the vortex forms and then breaks down. Some configurations have breakdown as low as 4° angle of attack.

A further investigation of the causes of vortex breakdown and the resulting quasi-periodic buffet is the purpose for the work of the present report. In the process of this investigation the HASC code was to be updated and used to predict some of the vortex characteristics. It was also used as a guide for locating some of the probes in the experimental spectral analysis. Several corrections were made to the HASC code, and a more accurate algorithm for predicting camber and leading-edge bevel effects was developed. These and other developments are discussed in this report. Further detail of the HASC code and the concepts of this report were presented by Dixon[2] at the AIAA Atmospheric Flight Mechanics conference in 1994.

2.0 Some Basic Concepts

For continuity some of the basic concepts of the Vortex analysis of the HASC code are presented here. More details of these concepts can be found in Reference 2. More elaboration on the final vortex burst is given in Section 2.2.

2.1 Vortex characteristics

2.1.1 Vortex Circulation and Entrainment

These characteristics are obtained from a Semi-empirical, two-dimensional analysis. Due to a unique method[1,2] of obtaining the equivalent two-dimensional angle of attack from the three-dimensional output, airfoil data can be used. Reference 2 shows the equations that use the loss of the airfoil leading-edge thrust to obtain the free vortex circulation and entrainment.

2.1.2 Vortex Core Size

Vortex core size is based on the mass flow entrained and is calculated from a continuity equation and pressure gradient equation given in Reference 2. The pressure gradient equation is a function of the circulation.

2.1.3 Vortex Position

Vortex position is obtained from an empirical concept given in Reference 2. The method accounts for leading edge flaps and/or bevels.

2.1.4 Vortex Stability

Two criteria are used to determine the breakdown of the laminar vortex. These are (1) A critical pressure gradient along the vortex axis (using 0.5), and (2) a critical vortex helix angle if the pressure gradient is at least 0.4. The difference between laminar vortex breakdown and the final vortex burst is discussed in Section 2.2

2.1.5 Vortex Burst

Vortex burst is the final chaotic condition of the spiral core. See Section 2.2.

2.1.6 Effect of Breakdown on Forces and Moments

When the laminar vortex breaks down the turbulent core become large, and as it crosses the wing trailing edge it affects the Kutta condition causing an effective loss in local angle of attack. An empirical method based on data from a large scale test[3] was developed to compute the effective loss in angle of attack. This is discussed in detail in References 1 & 2. A shift in the aerodynamic center is computed also to correct the moments.

When the final burst occurs equations developed for a totally stalled airfoil are used to compute the forces and moments on the wing sections affected by the burst. The wing sections affected are determined empirically as a function of their relative position to the burst.

2.2 Vortex Breakdown

2.2.1 Nature of Vortex Breakdown

For moderately swept wings the vortex breakdown goes through two stages. The first stage is the transition to a turbulent vortex which is the spiraling of the previously laminar vortex core. Then there is a final chaotic burst of this spiraling core. Prior to burst this previously laminar core is still coherent, but it becomes turbulent and it is now spiraling within an envelope that is called the turbulent vortex diameter. Uberoi[4] developed an equation for this diameter that is a function of the vortex circulation and distance from the origin of transition. This equation is used in HASC.

2.2.2 Sweep Effects

For delta wings with sweeps less than 70 degrees this turbulent vortex can exist all the way from the apex to the trailing edge without chaotic burst. The extent depends on the sweep and the angle of attack. As noted in section 2.1.6 the loads and moments are significantly affected, but not severely until the vortex burst.

As the sweep approaches 70 degrees, the axial distance between the turbulent transition and the burst gets smaller until the two are almost together at the trailing edge. For sweep angles greater than 70 degrees the distinction between transition and burst can not be found. The transition occurs, but it may immediately turn into a bubble type of burst.

Most of the early flow visualization tests were done with the wing sweep greater than 70 degrees; so this long transition of the vortex for the moderately swept wing was not even considered. Much was made of the bubble and spiral type breakdown, but it was not realized that this spiral could persist at lower sweeps and higher speeds than that observed in the water and smoke tunnel tests.

2.2.3 Effect of Negative Vortex Elements

At some spanwise position along the span, vortex elements that shed from the leading edge have negative circulation values; i.e., their circulation is the opposite sign of the free vortex. The explanation for this is that elements get their strength from the gradient of the vortex lift across the wing span. The vortex lift is increasing initially, but at some spanwise station it must start to approach zero at the wing tip. Therefore, where the vortex lift starts decreasing, the elements develop negative circulation.

The questions were: (1) What effect do these negative elements have on the free vortex stability, and (2) Do they decrease the free vortex circulation? The answer to these questions is still speculative, but some intuition and experimental results have been used to develop ways to include their effect in the HASC code.

On the basis of some early water tunnel observations the author has observed that these negative elements tried to wrap around the free vortex, but they were unstable. This could be the disturbance that triggers the laminar breakdown if the vortex is at a critical state. This trigger is possible for the high swept wings but not for the moderately swept wings. For the high swept wings these negative elements occur at a spanwise

station inboard of the initial breakdown span. On the wings with sweep less than 70 degrees transition has already occurred before the negative elements are shed. These negative elements do cause negative velocities along the vortex core encouraging the final burst.

2.2.4 Negative Elements and Negative Core velocities for the HASC Code

For the HASC code these negative elements are assumed to wrap around the free vortex, and this causes a negative velocity along the vortex axis. In Figure 1 the negative elements are shown wrapped around the free vortex of the 59.3 clipped delta wing that was used in most of the experiments for this program. Velocities are computed along the vortex axis from these elements and they produce a negative axial velocity.

An additional negative velocity is assumed to come from the core that is spiraling within the turbulent vortex diameter as described in Section 2.2.1. The velocity from this entity is empirically developed as a function the strength of this spiraling core. These velocities are added to the other induced velocities and the free stream component. The total becomes negative at some station, and when the velocity is -0.58 the vortex is considered as burst (chaotic). Axial velocities of around -0.5 just prior to burst have been observed by this author and others during laser velocimeter tests.

This value of axial velocity is approximately the same experimental level obtained by Leuchter & Solignac[4] when the vortex they were investigating burst. In this case burst was indicated by the turbulent intensity of the axial velocity that dropped rapidly to a relatively low level and almost constant value. As noted in Section 2.2.1, this where it is reasoned that the spiral of the turbulent core breaks up and turns chaotic. This reasoning comes from the concept that the spiraling, turbulent core is the primary source of the turbulent intensity; therefore, when it breaks up the turbulent intensity drops significantly. This is discussed further in the following section.

2.2.5 Experimental Justification

During the course of work for this program Georgia Tech graduate students provided experimental data that were directed to not only understand the quasi-periodic buffet phenomenon, but to an understanding of vortex transition and burst. Hot wire probes were used by Hubner[6] to obtain the frequency content and track the cause of the quasi-periodic forcing function. Laser velocimeter data were obtained by Hubner to help define the character of the vortex just prior to burst.

Flow visualization and hot wire spectral data by Hubner demonstrated that the rate of rotation of the spiraling core corresponded to the frequency of the quasi-periodic forcing function. This explains the high power of this forcing function and the confirms the character of the turbulent vortex. This phenomenon is observed in tests of small scale to full scale[7] such as found on the F-18 With this evidence it is concluded that the method of defining the turbulent vortex in the HASC code is well founded.

The character of the turbulent vortex just prior to burst was examined by Hubner on the 59.3 degree delta wing. Laser velocimeter mean velocities and the turbulence intensities as determined by RMS values were obtained. Figures 2 & 3 show

---

respectively the mean and RMS values of the velocities parallel to the root chord axis. For these figures two planes of data were taken just ahead of the root trailing edge. The third plane between these two is an interpolation.

The RMS results show that the highest turbulence intensity is in an annulus around the primary core. This is in agreement with the results found by other researchers such as those of Leuchter & Solignac[4] as noted in Section 2.2.4. This also is an indication that the spiralling of the pre-transition core is a major source of the quasi-periodic turbulence. As noted by Hubner and Komerath[6], there are other possible sources for the quasi-periodicity.

In spite of the turbulence, the vorticity analyses show a coherent vortex at these locations, but the vortex is about to burst. Burst occurs at a slightly higher angle of attack for the stations shown in Figures 2 & 3 or at stations slightly downstream at the angle of attack for Figures 2 & 3.

Although the mean velocity is positive on the centerline of the vortex core, the RMS and the histograms indicate negative velocities part of the time. This result says the vortex is about to burst. Force data shown in Figure 4 indicate the angle of attack at which this data was obtained (31 degrees) is at C_{Lmax}. This means that most of the lift deterioration is caused by the turbulent vortex effect on the Kutta condition as discussed in Section 2.1.6. It is not the ultimate burst. Since the vortex is about to burst its diameter is about at its maximum, and is affecting most of the wing span. This all adds up to a maximum lift condition.

Information gained from these tests was used as a guide to set the empirical factors in HASC so that the vortex burst at an angle of attack just above 31 degrees. Since HASC shows a higher C_{Lmax}, It appears that the effect of the turbulent vortex is not as severe in HASC as in the test. Alternately, the burst downstream may affect the forces and moments more than that set by HASC. Post burst values compare well for the lift, however. These results are discussed further in Sections 3.2 & 4.0.

3.0 Code Improvements

3.1 New Versions and Improvements for HASC

During the update of the HASC code three new versions of the code were released; i.e., 1.1, 1.2, and 1.3. The following was accomplished.

* Items done in version 1.1

** Items done in version 1.2

*** Items done in version 1.3

a. The HASC code has been set up to operate on a personal computer using the Silcon Valley Systems Fortran compiler. *

b. Several code errors have been discovered and corrected. * &**&***

c. The code has been modified to more accurately account for the effect of turbulence on the loading and total aerodynamic forces and moments. *

d. New equations were introduced to improve the calculation of lateral-directional forces and moments.* &**

e. A major change in computing the camber effects now allows accurate accounting for small leading and trailing-edge deflections, bevels, and other camber devices. These devices have significant effects on vortex characteristics.* &**

f. Several corrections were made to the tail contributions allowing the vortex flow characteristics and effects to be included. **&***

g. Due to the inability of the original code to compute the effects of multiple and merging vortices on vortex stability the effect of multiple vortices has been incorporated in version 1.2 &1.3. The subroutine, VORSYA, that calculates these effects is considerably improved in version 1.3.**&***

h. Version 1.3 now includes a better routine to predict the final burst of the vortex; i.e., from initial turbulent or spiral breakdown to chaotic burst. A reverse flow along the free vortex axis is now computed. When velocity reaches a value of -0.58 the vortex burst, and loads are affected accordingly.***

i. To accomplish section 2.1.h, subroutine REVFLO in version 1.3 computes the effect of vortex elements shed from the leading edge on the free vortex axial velocity. Only the elements that create negative circulation are included in the calculation. For one selected angle of attack the track or position of these elements can be found in the output of UNIT 100 (vorelmt.trk). This file gives: (1) the angle of attack, (2) the spanwise station (2y/b) where the element is shed from the leading edge, (3) the circulation of the element, (4) the X, Y, Z components of velocity, (5) the center line of the free vortex (XD,YD,ZD), and the coordinates of the track of the element (XR,YR,ZR). The angle is selected by the number of the angle of attack provided in the file VORLIF17.INP, and it is called LALXP. Currently it is set as the 13th angle as given in the main input file. This selected angle will be part of the main input in a later version of the code.***

3.2 Input and Output Comments

The appendix of this report gives details of the changes in output of the HASC code. No new input is required over the original code, but some caution is appropriate. Important comments are given in this section. These comments are a supplement to the appendix.

3.2.1 Input Angle of Attack

When running the code to get vortex effects (Surface type 1 & 2), some caution is required in specifying the input angles of attack. A history of the vortex breakdown is included in the VORLIF (Run for surface type 1 & 2) part of the code. It is reasoned that as angle of attack increases and vortex breakdown has occurred the breakdown will continue to occur at the wing stations where it occurred at lower angles. Also, the breakdown will continue to move inboard as the angle of attack increases. This means that your lowest input angle should not indicate breakdown. If it does, then you should rerun the code starting at a lower angle. You can tell if the breakdown has occurred by checking the output file STABCRIT.DAT. Look for the ratio of laminar vortex diameter to turbulent vortex diameter, RADR. If it is less than 1.00 breakdown has occurred. Note: Cycle 2 and 3 results are given in STABCRIT.DAT. RADR will be less than 1.00 only in the 3 cycle which the second or last part of the output for each surface

Further caution is emphasized in the appendix for the proper angle of attack input. The angle of zero lift should be included in the input.

3.2.2 Effect of Number of Spanwise Stations

Some effect of the number of spanwise stations may occur when the vortex breakdowns. Currently the code will not allow the initial vortex transition to occur at or inboard of the fourth span wise station of each vortex. The reason for this is that in the starting process there are numerical instabilities, and it takes 3 to 4 stations for this to settle. This means that the effect of the turbulent vortex on the loads may be less according to the code than it really is. An example of this is the code C_{Lmax} output of Figure 4 compared to the test results for the 59.3 delta wing. As shown in the figure more spanwise stations tend to correct this problem. Note: This problem occurs every where a break in the leading edge causes a vortex to form.

This anomaly may be corrected by more spanwise stations or by paneling of the surface so that the first four stations of the vortex are confined to a small part of the span at the apex of the vortex. If this is done, at least two panels of equal width should be added near the apex so that the first four stations are on the inboard panel, and only 2 stations are on the second, outer panel. These panels should be no more than 10% of the span in width. This will keep the four stabilizing stations inboard of the 10% span, and not have large jumps in the spacing of the spanwise stations. This should improve the results discussed in Section 4.0

4.0 Analytical Development of Stall and Post Stall

At the angles of attack near stall and at post stall, empirical factors that account for viscous effects must be examined for several configurations. One of these configurations was the 59.3 degree delta wing investigated by Hubner[6] for which some discussion is presented Section 2.2.5. The next configuration is a 63.03 degree delta wing[3]. A third configuration is the aspect-ratio-one Hummel[8] wing. When any changes were made in the empirical factors to improve the output of any one of these

configurations, the other two configurations had to be investigated for compatibility of the change.

4.1 Force and Moment Data

4.1.1 The 59.3 Degree Clipped Delta Wing

The laser velocimeter data of Figures 2 & 3 indicate the vortex is on the verge of bursting at an angle of attack of 31 degrees for the 59.3 degree wing. It is assumed that the burst occurs at all higher angles. Therefore, the empirical parameters are set for the burst to occur at the next angle run in the HASC code. As noted in the previous section the analytical C_{Lmax} in Figure 4 is much too high for the 20 spanwise station model, but much better for the 26 spanwise station model. The error in C_{Lmax} is less than 6% for the latter. The post stall looks good in both cases, but is slightly better for the latter. Paneling as suggested in Section 3.2.2 should improve the results even more without requiring a large number of spanwise stations.

There are anomalies in the results for both the pitching moment and the drag. It is believed that because the force testing system used for the 59.3 degree wing is relatively new there some additional blockage and data reduction corrections that need to be made.

HASC predictions of the pitching moment for the 59.3 degree wing appear to have a shift in the aerodynamic center of about 4.5% downstream relative to that of the test data. There are two reasons that the center of gravity, CG, of the test data may be in error. First, as shown in Figure 4, the HASC CG location was moved aft 4.5%. At all the angles of attack this caused the moment to agree very well with the test data except right at C_{Lmax}. Second, the pitching moment has been agreeing well for other configurations when the CG is known to be correct. If empirical adjustments were made to the aerodynamic center of the HASC code, the pitching moment of the 63.03 degree delta wing of Figure 5 would be inaccurate.

The zero lift pitching moment, C_{M0}, predicted by HASC is in excellent agreement with the test data. Some caution must be given at this point. The C_{M0} is sensitive to the bevels at the leading and trailing edge. The proper way to input these bevels is given in the Appendix, but viscous effects must be considered also. For the 59.3 degree delta wing the boundary layer thickness grows enough at the inboard end of the wing to wipe out the effect of the trailing edge bevel at the wing root. This effect is progressively less as the wing tip is approached. For input to the HASC code the bevel was assumed to have zero deflection inboard and full defection outboard. If the bevel had been on the upper surface, the boundary layer effect would probably not be as significant, because the free vortex down wash effect is compensating.

Compensation for the viscous effects just discussed will require some knowledgeable judgment. Each configuration may be different. For example no correction was applied to the trailing edge bevel angle of the Hummel configuration shown in Figure 6. The reason for this is that the forward bevel extends well back towards the trailing edge.

This produces a slightly favorable pressure gradient so that the boundary does not build up to wipe out the trailing bevel.

As with the pitching moment the drag of HASC and the test data have some differences. HASC has normally been giving very accurate values of the drag as can be seen in the Hummel wing comparison of Figure 6. Therefore, as noted above some additional blockage corrections are required for the test data.

4.1.2 The 63.03 Delta Wing

When any changes are made in the empirical factors to match the test data, these changes are evaluated on the 63.03 degree wing. Since this wing was tested at nearly full scale Reynolds number and comprehensive pressure data were available, this configuration is considered a baseline. Figure 5 shows the lift and pitching moment of this configuration compared with the HASC code output. As can be seen the changes in the empirical factors made for the 59.3 degree wing are compatible with the output for the 63.03 degree wing.

4.1.3 The Hummel wing

The Hummel wing[8], shown in Figure 6, is a high-swept, aspect-ratio-one wing with camber due to beveling on the lower surface. With all the empirical parameters the same as those of the 59.3 and 63.03 degree wings, good results are obtained with the HASC code. Some improvements in the stall range for all three components could be made, however. These high sweep configurations have the free vortices so close together that their mutual interference effects have not been fully captured in the HASC code.

The free vortices are not currently represented in the basic vortex lattice part of the code. This is a major change, but should be done to eliminate some of the empiricism that is presently required for these high swept delta wings. This will also improve the cases where multiple vortices such as formed by a strake and wing combination. This improvement is the subject of a future version of the code.

5.0 Application of the HASC Code to Buffet

As noted previously the quasi-periodic forcing function (buffet) has been a major concern of this effort. In Section 2.2.5 it was noted that the rate of rotation of the spiraling core corresponded to the frequency of the quasi-periodic forcing function. This phenomenon was expected when it was discovered that the reduced frequency of this quasi-periodic forcing function could be defined using the turbulent vortex diameter as follows:

$$\frac{fD_v}{V_\infty} = 0.5 \qquad (1)$$

The turbulent vortex diameter, D_V, was computed by the HASC code. Combining that with the experimental frequency, f, and the free stream velocity, V_∞, the reduced frequency was equal to the constant of 0.5 as in equation (1). These results are shown in Figure 7 for the 59.3 degree delta wing at angles of attack of 18 and 30 Degrees.

The experimental data were obtained with a hot wire probe at stations along and just above the leading edge. These are plotted as a function of the longitudinal body axis, X, normalized by the root chord, C_O. The analytical results were obtained at X/C_O of the outer edge of the vortex core, which is very close to the leading edge.

At both angles of attack of the figure an arrow point to the position where the HASC code has predicted transition of the vortex. The arrow noted as laminar is the last position for which the code showed the vortex as laminar. The lower arrow points to where the code first predicts fully turbulent vortex. As can be noted there is no experimental quasi-periodic function until after the vortex transitions to turbulence; i.e., the laminar core begins to spiral. This spiral rotates within the envelope of the predicted turbulent core; so, the rate of rotation or the frequency scales with the vortex diameter. Note: In the figure the reduced frequency is scaled by the mean chord as normally done for most test data.

The X distance between the arrows of the laminar and fully turbulent vortex is not necessarily the transition distance, but appears to be that for the 30 degree results. The experimental quasi-periodic frequency begins at the last predicted laminar vortex position. Also, the peak power that corresponds to the quasi-period frequency begins to rise at this position. The power then starts to drop near the predicted position of fully turbulent vortex. This seems very logical that the power would increase as the vortex transitions to the fully turbulent position; i.e., the vortex core size is growing and the turbulence is increasing very rapidly during the transition. Then the vortex grows at a much slower rate, and the strength of the spiral is probably decaying.

The HASC code does not gradually increase the vortex core size between the last laminar and the fully turbulent positions. If it did, the hump in the analytical curve between these positions would be smoothed. There is a hump in the analytical curve for the 18 degree case also. Unfortunately, the transition for the latter is well ahead of that for the experimental results. Also, this early prediction causes the turbulent vortex diameter to be larger than it would be for a delayed prediction. A delayed prediction would raise the reduced frequency, and probably produce better agreement with the experimental frequency.

The main discovery is that for either the 18 or 30 degree case the predicted reduced frequencies agree well with the experimental values once the vortex has become fully turbulent. Any surface downstream of the origin of the turbulent vortex will experience severe buffet at frequencies predicted by the code.

6.0 Conclusions

A better understanding of the interaction of vortex flows and their effects on the forces and moments on a configuration dominated by vortex flows has been obtained. This understanding comes from a combination of analytical and experimental investigations. The knowledge gained has been incorporated in the HASC preliminary design code with typical improvements as follows.

1. A more reliable and much improved version 1.3 of the HASC code has been developed.

2. The effects of camber and edge bevels are accurately predicted. This includes the differences between upper and lower bevels.

3. The mutual interference of multiple vortices has been greatly improved. Some additional effort in future versions is needed for this phenomenon. Currently, empiricism is required to account for merging vortices.

4. Vortex breakdown and burst analysis is greatly improved. The understanding of the initial breakdown (transition and spiralling of the laminar core) was enhanced by the experimental work. Final burst (chaotic breakdown of the spiraling core) is analyzed more accurately for the HASC code

5. It was discovered that the turbulent vortex core diameter can be used as the scaling term in the reduced frequency for a quasi-periodic forcing function. This function is one of the causes of major buffet loads on surfaces in the vortex wake. The reduced frequency is equal to 0.50, and this appears to be a universal constant.
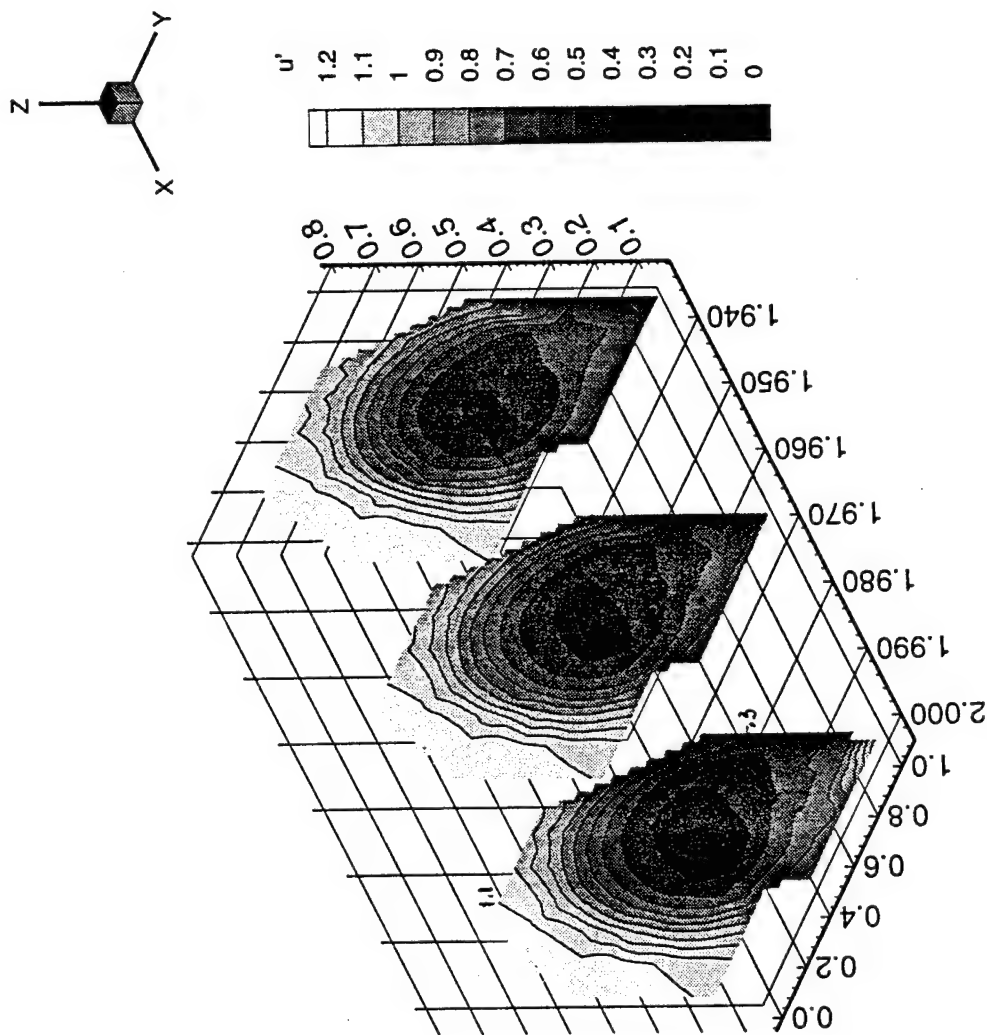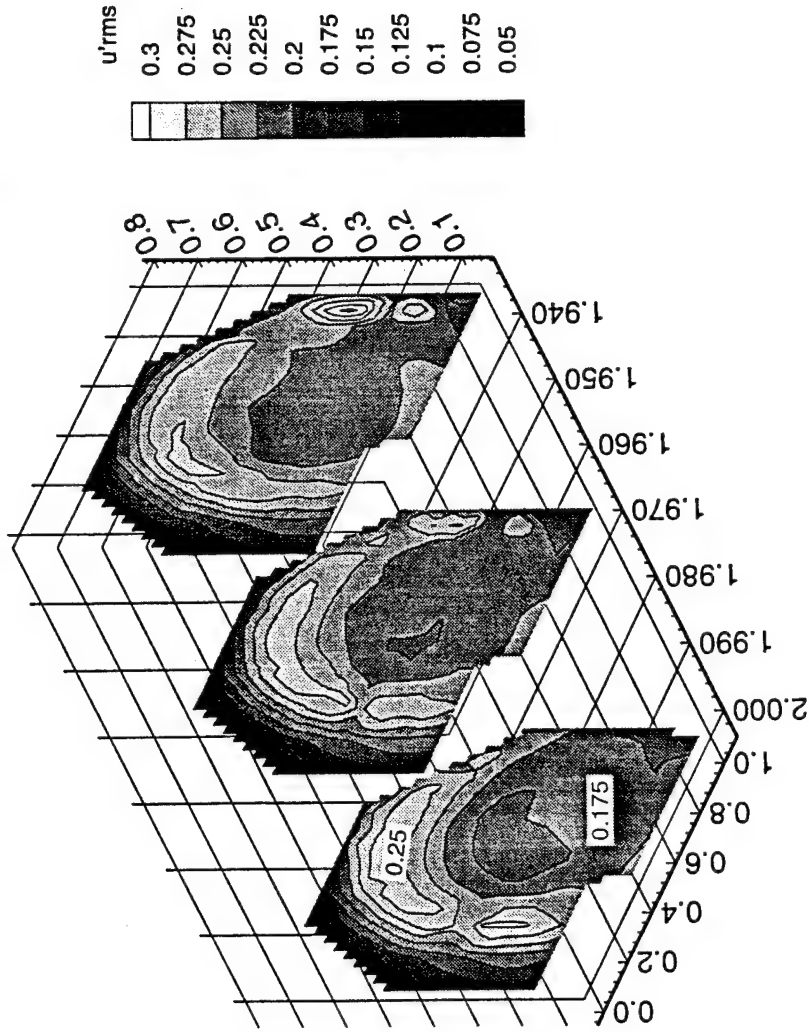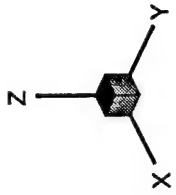
7.0 References

1. Adler, C. O. & Dixon, C. J., "High Angle of Attack Stability and Control -- Prediction Methods and Code," Air Force Report, WL -- TR-92-3050, October 1992

2. Dixon, C.J., "Semi-Empirical Analysis of Vortex Breakdown with Aerodynamic and Buffet Effects," AIAA Paper 94-3483, August 1994

3. Anderson, A.E., "Chordwise and Spanwise Loading Measured at Low Speeds on Large Triangular Wings," NACA RM No. A9B17, April 19, 1949

4. Uberoi, M. S., "Mechanisms of Decay of Laminar and Turbulent Vortices," Journal Fluid Mechanics, Vol. 90, part 2, pp. 241-255,1979

5. Leuchter, O., & Solignac J. L., "Experimental Investigation of the Turbulent Structure of Vortex Wakes," ONERA T.P. n° 1983-107, Presented at the University of Karlsruhe, Sept. 12-14, 1983

6. Hubner, J. P., & Komerath, N. M., "Spectral Mapping of Quasi-Periodic Structures in a Vortex Flow," <u>Journal of Aircraft</u>, Vol. 32, No 3, p 493, May-June 1995

7. Meyn, L. A., & James, K. D., "Full Scale Wind Tunnel Studies of F/A-18 Tail Buffet," AIAA Paper No. 93-3519, Presented at the AIAA Applied Aeronautics Conference, August 9-11, 1993, Monterey, CA

8. Hummel, I. D., "On the Vortex Formation Over A Slender Wing at Large Angles Of Attack," AGARD- CPP- 247, <u>High Angle of Attack Aerodynamics</u> AGARD -- FDP Symposium, Sande F' Jord 1978, pp 15-1 -- 15-17
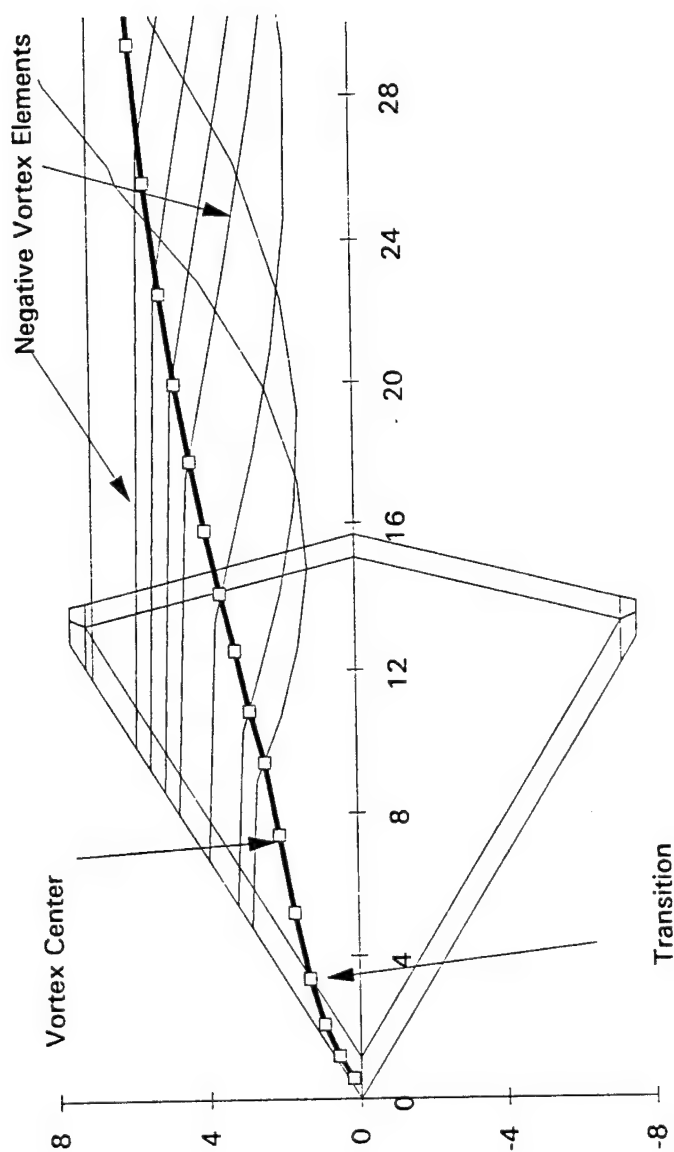
Figure 1 Vortex Center and Negative Vortex Elements
59.3 Delta Wing, Alpha = 31 Degrees
Page 14

Figure 2   Contours for the Mean U Component of Velocity in Trailing Edge Planes
- 59.3 Degree Delta Wing at 31 Degrees Angle of Attack-

Page 15

Figure 3 Contours for the RMS of the U Component of Velocity in Trailing Edge Planes

- 59.3 Degree Delta Wing at 31 Degrees Angle of Attack -
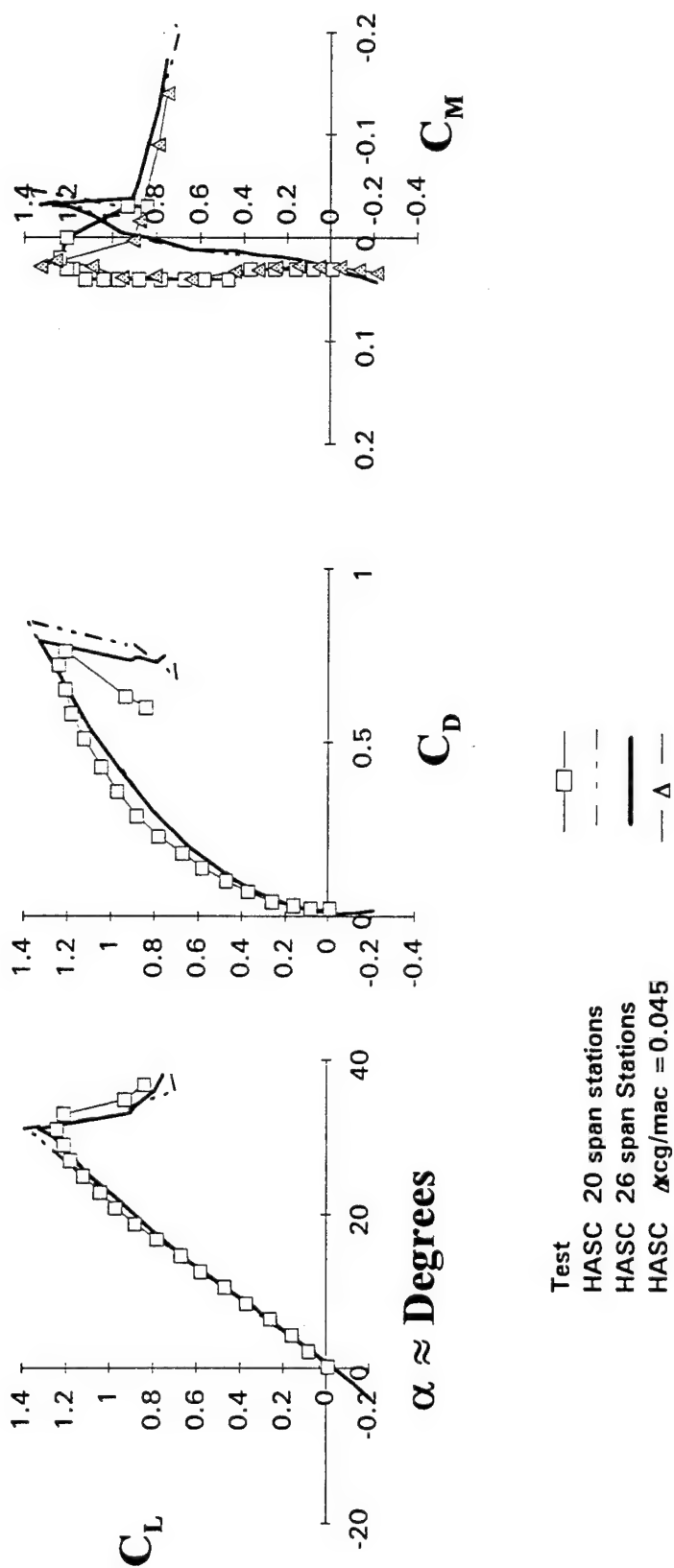
Page 16

Figure 4 Analytical and Test Aerodynamic coefficients
for
59.3 Degree Swept Cropped Delta

Page 17

Figure 5 Analytical Versus Test for 63.03 Degree Delta Wing

Page 18
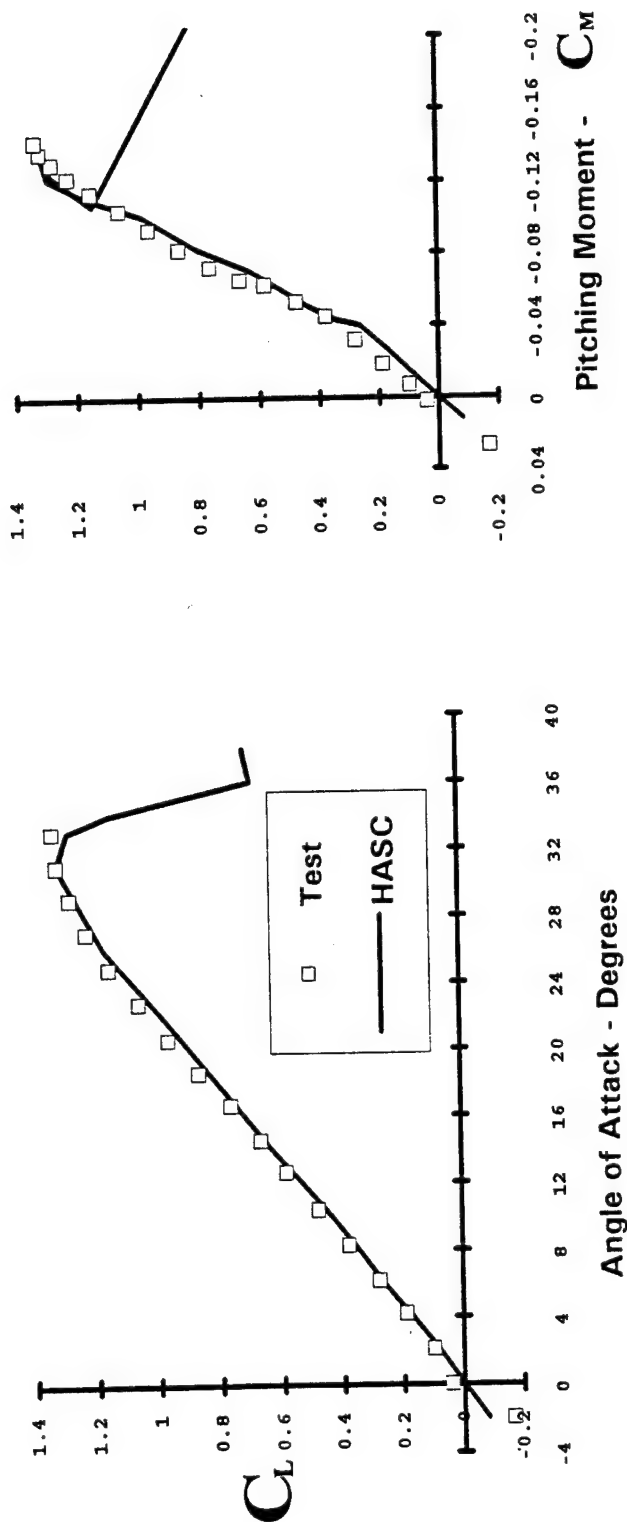
Cl & Cd

Cd

CL

Angle of Attack
-Degrees-

-12   -4   4   12   20   28   36

1.2
1
0.8
0.6
0.4
0.2
0
-0.2
-0.4
-0.6

Ledgend: Test - ○ ; Hasc   ———; Vorlax -△-

Cm

-12   -4   4   12   20   28   36

0.15
0.1
0.05
0
-0.05
-0.1
-0.15

-0.8 -0.6 -0.4 -0.2 0 0.2 0.4 0.6 0.8

0
0.2
0.4
Meters 0.6
0.8
1

Airfoil is flat upper surface
with
beveled lower surface
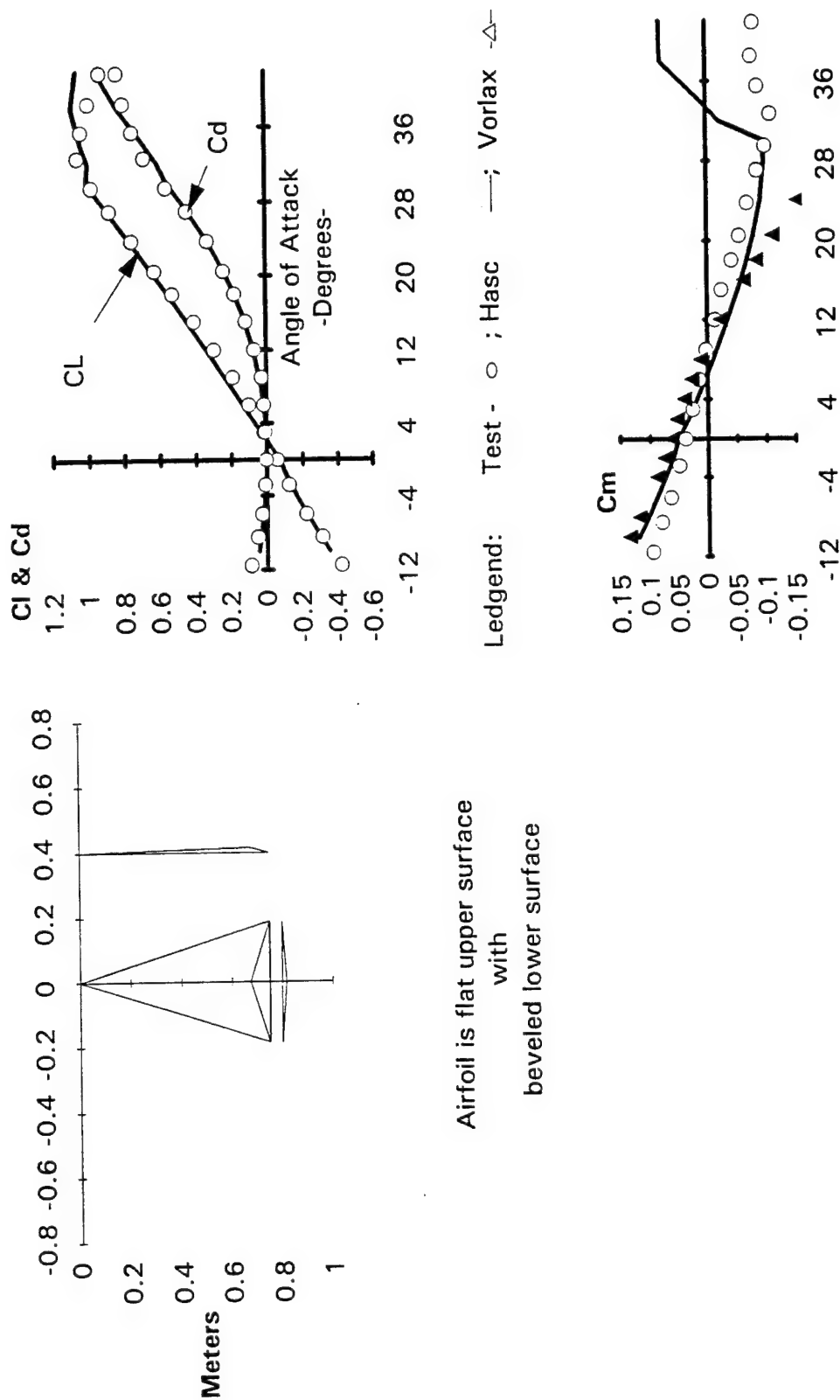
Figure 6 Hummel Aspect Ratio One Wing -- Analytical and Test
Page 19

Figure 7 Analytical and Test Buffet Reduced Frequency and Test Peak Power
-59.3 Degree Clipped Delta Wing-
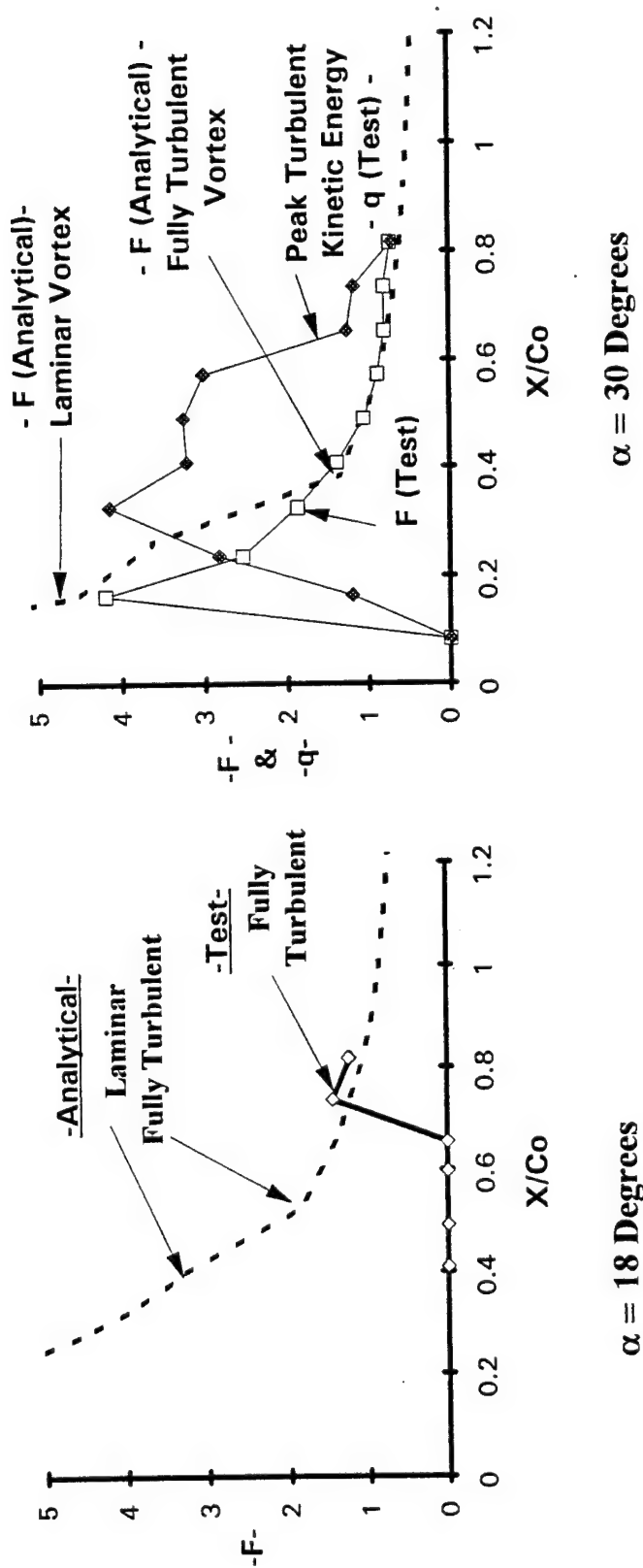
Reduced Frequency $\qquad$ $F = fC_{avg} / V_\infty$

Peak Power $\qquad$ $q = (rms / 10\, V_\infty)^2$

Page 20

Appendix

HASC Code Version 1.3
"Changes in HASC code from version 1.0, 1.1, and 1.2"

1.0 Overview of Improvements in the HASC Code

The HASC code now has many improvements to make it more accurate and reliable. The following provides the changes in the code. There are no changes in the basic input except the input file names. Some clarifications of certain input terms are given. New output data and files are discussed.

2.0 File Opening

a. HAS1.FOR is the main program, and file opening statements are now included in this module.

b. All the files listed in the original report, WL-TR-92-3050 are included.

c. A new file is opened in unit 28 to print the predicted frequency for the peak unsteady aerodynamic forcing function. This output will be discussed in Section 4b.

d. A new file is opened in unit 85 to provide a table of the planform coordinates to use in a spread sheet for plotting. This was improved in version 1.2.

e. A new file is opened in unit 100 to provide a table of the coordinates for the negative vorticity elements shed from the leading edge. This is discussed in Section 1i and it is in version 1.3.

f. The number of files allowed to be opened is set by an $SVS**C^3$ function found just after the common statements in HAS1.FOR. It is set now for 103 files. For other compilers the call for this function will have to be deleted.

3.0 Input Changes and Clarification

Caution: note the original HASC report input error in step 3g. Also, note the canard and tail length input in 3d.

a. The basic configuration input file, unit 15, must be called CONF.HSI.

II-21

b. The airfoil definition file, unit 3, must be called CONF.AFI. This file must be created if non-standard NACA airfoils are used on surfaces (SRTYP 2) where vortex flow analysis is desired. Some clarification of this file and its relation to the panels that use the airfoils is given here.

A new panel should start where the type of airfoil changes or where breaks occur at the leading or trailing edge of the wing or lifting surface. Also, panels on upstream or downstream surfaces must have the same spacing.

Some caution in defining the airfoils for panels used for leading or trailing edge flaps is necessary. For these types of panels the most aft panel (e.g., trailing-edge flaps) should be input first, and then each succeeding panel towards the leading-edge. The airfoil flag, IARFYL, should be set to 1 or 2 for the leading-edge flap panel and to 0 for the aft panels. Use 1 for airfoils of known leading-edge radius and thickness and 2 when the airfoil definition file is used.

c. The choice of Input angles-of-attack is not as critical as version 1.1 for a cambered or twisted planform or for a planform with incidence relative to the Fuselage Reference Line, FRL; e.g., a horizontal tail at incidence. The code will probably be more accurate if each wing section zero lift angle (value computed by VORLAX) is included in the chosen three-dimensional angle-of-attack range. Check the output file CONF.VOT for the sectional zero lift angle of attack computed by VORLIF. If desired, unit 82 can be mobilized to print sectional values for both VORLAX and VORLIF.

The code now searches the entire angle-of-attack range for the geometric (value computed by VORLAX) zero-lift angle of attack, α_{0l}, for each wing section. The code then uses all the input values of the angle of attack up to two angles above α_{0l} to define the equivalent two-dimensional zero-lift angle of attack and the local lift curve slope. It is not critical, but slightly more accurate values will be obtained for these parameters if α_{0l} occurs within the first 6 chosen angles of attack. A guess must be made for α_{0l}, and at least one angle input a couple of degrees or less below α_{0l}.

Both the wing and tail or canard α_{01} values must be considered. For example; if the tail incidence is 10 degrees nose up and the α_{01} for the wing is 4 degrees, a good choice of the first 6 angles of attack will be -12, -8, -4, 0, 4, 6. The rest of the 14 allowed angles can extend the calculations past stall.

If the only the VORLAX part of the code is run (SRTYP = 5), the choice of angles is not sensitive as noted above, but no vortex breakdown analysis will be made.

d. For clarification, the tail or canard moment arm (tail length), FTAIL, is the distance from the center of gravity to the aerodynmic center of the aft surface. It is positive in the aft direction, and it is normalized by CBAR. This works for either a tail or canard configuration. The value for FTAIL must be input for the forward surface which is always a type 2, if vortex analysis is required. For canard configurations the canard is type 2, and the wing is type 1.

Caution: All type 1 or 2 surfaces must be input in the order they appear in the plan view of the configuration from forward to aft; e.g., SURFACE 1 is left canard, SURFACE 2 is right canard, SURFACE 3 is left wing, and SURFACE 4 is right wing. All other type surfaces can appear before or after the type 1or 2 surfaces.

e. For missile configurations with bodies that are large compared to lifting surfaces, some experimentation is suggested. In the forebody definition set the fuselage length, FSLNTH, to extend all the way to the wing even if there is a canard, and use this entire length in the VTXCLD calculations by setting FSLINC equal to 1.0. For the rest of the body, use VORLAX type of calculation by setting SRTYP to 5. For sideslip calculations be sure to include a vertical flat plate projection of the body in both VTXCLD and VORLAX type input; i.e., SRTYP 3 & 5 respectively.

f. The effect of different beveled leading edges can be incorporated, where vortex flow analysis is to be made (SRTYP 2). Some wind tunnel models have the leading edge beveled only on the windward surface, some are beveled only on the leeward surface, and some are symmetrically beveled.

To simulate the bevel on only one side, the airfoil is input as a symmetrical bevel in the airfoil definition file, unit 3, with the beveled angles at one half the angle of the actual angle. The beveled portion of the wing then becomes a leading edge flap that is input as a panel deflected at one half the actual bevel angle. The deflection is given a negative value if the bevel is leeward and positive if it is windward.

The vortex characteristics are sensitive to these small camber and leading-edge slopes. HASC now accounts for these effects.

g. Caution: If the airfoil is a standard type and camber is also input, the original HASC report is in error for the sequence of these two inputs. The airfoil definition must be input first; i.e., card 11. The camber must follow as cards 12 to 14. Also, no two consecutive chordwise camber ordinates can be equal. They must be different in the fourth decimal place, at least. This also means that zero camber can not be input at one end of a panel where the other end has finite values. Very small values in the fourth decimal place will work, however.

h. The vortex cloud code, VTXCLD, is now in (4) sub codes: VTXM, VTX1, VTXCL2, & VTXPLT. If VTXCLD plotting of the vortices is not required, use only the first two sub codes. If plotting is desired use VTXM + VTXCL2 or VTXM + VTX1 +VTXPLT. In either case the source code VTXM must be changed at the locations marked by "CJD" to call for the plotting.

4.0 Output Changes

a. The main output files will be named CONF with a three letter extension corresponding to the type output. For example, CONF.HSO is the main force and moment output for the total configuration and each surface. CONF.VOT gives section data for VORLIF calculations. In other words CONF replaces the wild card * in the file names of the original report.

b. The new file in unit 28 is named VPOSFQ.OUT. The predicted reduced frequency, $f\ C_{avg}/V_o$, for the peak aerodynamic forcing function is given as a function of the location of the inner and outer vortex core edges. This

frequency is the same on the inner and outer edges. It is computed from the following equation:

$$f\, C_{avg}/V_0 = 0.5\, C_{avg}/D_v$$

where D_v is the computed vortex core diameter, f is the frequency(Hz), and C_{avg} is the average wing chord. The value of ($f\, C_{avg}/V_0$) is valid only where the vortex is turbulent; i.e., where R_{lam}/R_{turb} is less than 1.0.

c. Several write to screen statements have been added just to watch the progression of the code. These may be removed if desired.

d. Note the new output in unit 100 discussed in Sections 1i & 2e

5. New Input for Tail Contribution

a. It has been determined that the effective tail incidence is smaller than the VORLAX results. The reason for this is that VORLAX uses a "venetian blind" effect to compute the slope of the airfoil; i.e., each control point or panel along the chord is assumed to be at the incidence angle. This tends to create more fuselage lift carry over the actual case. A span factor has been included in VORLIF to compensate for this problem.

The factor used, called BLAMDA, is computed according to the familiar flap span factor developed by Lowry & Polhamus, Reference 1. This factor is computed by assuming tail lift carry over is 1/2 of the fuselage width. Multiplying the actual tail incidence angle by BLAMDA gives the effective tail incidence.

The only input required is the taper ratio of the tail. The term is BLAMX found in the unit 17 input, VORLIF17.INP, If you want the effective incidence computed, input the actual taper ratio for this term. If you want no correction, input -1.0. Currently it is set at a value of 0.5 which approximates most tail taper ratios. Actual values of taper ratio from 0.0 to 1.0 can be input. BLAMDA will change but it is not very sensitive to the taper ratio.

6.0 Effect of Multiple and Merging Vortices

a. In general the theory for multiple or merging vortices were not included in versions 1.0, & 1.1 of the code. Version 1.2 has some effect of the mutually induced velocities of multiple vorticies Version 1.3 has a much improved multiple vortex effect. No version will merge the vortices. This is planned for a future version. For now some of these effects are accountable by a simple change in the critical pressure gradient, GRADT, for breakdown of the laminar vortex. For burst of the turbulent vortex the critical average axial vortex core velocity, VABR, is changed.

For wings with no fuselage the vortices from the right and left wings have a favorable effect on each other. The critical pressure gradient for wings with sweep of 65 to 76 degrees is allowed to increase from 0.5 to 1.0 respectively. The value of GRADT remains at the basic input (CBFACT) of 0.5 for wings with fuselage.

For merging vortices like the strake and wing vortex on the F16 there is a detrimental effect on vortex break down. GRADT is made to decrease for these kinds of vortices. To experiment with this change, either change GRADT in the VORLIF module or the input value of CBFACT. Note: GRADT is proportional to CBFACT

7.0 Empirical Factors Input

a. All empirical factors for vortex flow effects such as CBFACT, BLAMX, and VABR are found in unit 17, VORLIF17.INP. They are also "Hard Wired" into the VORLIF module. Since you may want to experiment with the above parameters, VORLIF is set so that the "Hard Wired" values are commented out of operation, and Read(17,--) is operating.

8.0 References:

1. Lowry, John G. and Polhamus, Edward C.: <u>A Method for Predicting Lift Increments Due to Flap Deflection at Low Angles of Attack in Incompressible Flow,</u> NACA TN 3911, January, 1957